sustainability

MDPI

Article

Enhancing Daylight Comfort with Climate-Responsive Kinetic Shading: A Simulation and Experimental Study of a Horizontal Fin System

Marcin Brzezicki

Faculty of Architecture, Wrocław University of Science and Technology, 50-370 Wroclaw, Poland; marcin.brzezicki@pwr.edu.pl

Abstract: This study employs both simulation and experimental methodologies to evaluate the effectiveness of bi-sectional horizontal kinetic shading systems (KSS) with horizontal fins in enhancing daylight comfort across various climates. It emphasizes the importance of optimizing daylight levels while minimizing solar heat gain, particularly in the context of increasing energy demands and shifting climatic patterns. The study introduces a custom-designed bi-sectional KSS, simulated in three distinct climates—Wroclaw, Tehran, and Bangkok—using climate-based daylight modeling methods with the Ladybug and Honeybee tools in Rhino v.7 software. Standard daylight metrics, such as Useful Daylight Illuminance (UDI) and Daylight Glare Probability (DGP), were employed alongside custom metrics tailored to capture the unique dynamics of the bi-sectional KSS. The results were statistically analyzed using box plots and histograms, revealing $UDI_{300–3000}$ medians of 78.51%, 88.96%, and 86.22% for Wroclaw, Tehran, and Bangkok, respectively. These findings demonstrate the KSS's effectiveness in providing optimal daylight conditions across diverse climatic regions. Annual simulations based on standardized weather data showed that the KSS improved visual comfort by 61.04%, 148.60%, and 88.55%, respectively, compared to a scenario without any shading, and by 31.96%, 54.69%, and 37.05%, respectively, compared to a scenario with open static horizontal fins. The inclusion of KSS switching schedules, often overlooked in similar research, enhances the reproducibility and clarity of the findings. A physical reduced-scale mock-up of the bi-sectional KSS was then tested under real-weather conditions in Wroclaw (latitude 51° N) during June–July 2024. The mock-up consisted of two Chambers '1' and '2' equipped with the bi-sectional KSS prototype, and the other one without shading. Stepper motors managed the fins' operation via a Python script on a Raspberry Pi 3 minicomputer. The control Chamber '1' provided a baseline for comparing the KSS's efficiency. Experimental results supported the simulations, demonstrating the KSS's robustness in reducing high illuminance levels, with illuminance below 3000 lx maintained for 68% of the time during the experiment (conducted from 1 to 4 PM on three analysis days). While UDI and DA calculations were not feasible due to the limited number of sensors, the E_{h1} values enabled the evaluation of the time illuminance to remain below the threshold. However, during the June–July 2024 heat waves, illuminance levels briefly exceeded the comfort threshold, reaching 4674 lx. Quantitative and qualitative analyses advocate for the broader application and further development of KSS as a climate-responsive shading system in various architectural contexts.

Keywords: kinetic shading systems (KSS); daylight comfort; climate-based daylight modelling (CBDM); sustainable building design; visual comfort; adaptive building facades; environmental control systems

check for updates

Citation: Brzezicki, M. Enhancing Daylight Comfort with Climate-Responsive Kinetic Shading: A Simulation and Experimental Study of a Horizontal Fin System. *Sustainability* **2024**, *16*, 8156. https://doi.org/10.3390/su16188156

Academic Editors: Jacopo Gaspari, Laura Aelenei and Lia Marchi

Received: 17 July 2024
Revised: 11 September 2024
Accepted: 12 September 2024
Published: 19 September 2024

Copyright: © 2024 by the author. Licensee MDPI, Basel, Switzerland. This article is an open access article distributed under the terms and conditions of the Creative Commons Attribution (CC BY) license (https://creativecommons.org/licenses/by/4.0/).

1. Introduction

Buildings account for about 40% of global energy use [1]. As the shift to renewable energy is a worldwide endeavor, achieving the goal of 100% clean energy still remains a question for the future. This means that every effort to cut energy use reduces carbon

emissions and helps meet climate goals, like Goal 7: Affordable and Clean Energy, issued by the United Nations in 2015 as part of the 2030 Agenda for Sustainable Development [2].

1.1. Background

As greenhouse gases accumulate, our global climate undergoes unprecedented shifts, leading to new weather patterns and more frequent extreme events [3]. While emissions reduction is crucial, climate change has triggered significant consequences, including storms, droughts, rising sea levels, and unpredictable temperatures. Given the climate system's inertia, these effects will persist, making it essential to develop climate-responsive design solutions. This involves optimizing building designs and urban planning to adapt to evolving conditions, enhancing sustainability. We can mitigate extreme weather impacts and ensure resilient, sustainable environments by integrating adaptive strategies, such as responsive shading and energy-efficient technologies.

1.2. Solar Energy and Daylight

Solar energy, comprised of almost equal amounts of light and heat (50% visible light—approximately 400–750 nm, 45% infrared radiation—750 and beyond nm, 5% ultraviolet 100–400 nm), offers a unique opportunity to save energy. Managing daylight effectively can significantly reduce direct sunlight entering buildings, lowering the heat gain and need for air conditioning. This not only improves comfort for occupants but also reduces energy costs. Furthermore, using energy-efficient technologies and smart design in architecture can enhance daylight use. Shading devices can help buildings manage light and temperature effectively, promoting sustainability and reducing carbon footprint on lighting and cooling.

Daylight is essential for human functioning, regulating circadian rhythms, and stimulating the production of hormones and vitamins. In the workplace, daylight is generally seen as a benefit for visual comfort, though excessive direct sunlight can cause glare and overheating. Scientific consensus holds that direct sunlight on the work plane should be minimized. For instance, the LEED 4.0 standard calls for the demonstration "through annual computer simulations that annual sunlight exposure ($ASE_{1000,250}$) of no more than 10% is achieved" [4]. Modern office buildings often feature floor-to-ceiling glazing, which can lead to excessive sunlight exposure, especially in south-facing rooms. To mitigate this, shading systems are employed to limit direct sunlight while ensuring adequate diffused light.

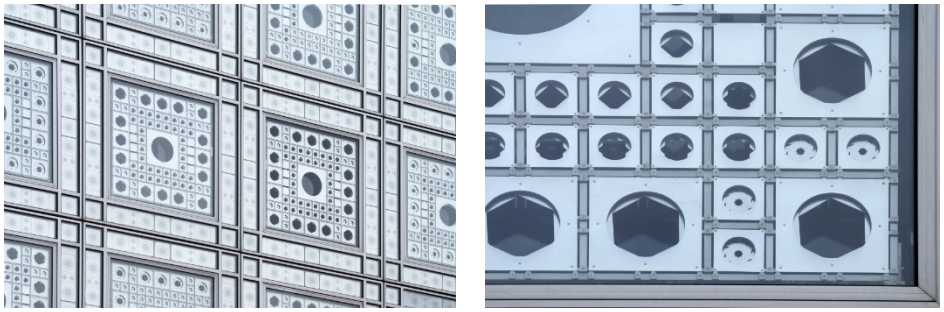
1.3. Kinetic Shading Systems in Architecture

Shading systems have been integral to building design, reflecting efforts to control indoor lighting. Solutions range from simple curtains to advanced Venetian blinds, but these often require manual operation. In the 1970s, adaptive facades emerged, enabling automated responses to environmental conditions [5]. These systems effectively regulate daylight and have become widespread in building design. Adaptive facades include technologies like glazing with adjustable transparency and adaptive wall insulation. Kinetic shading systems (KSS) are notable within this category, using mechanical elements to regulate sunlight, as exemplified by the mechanical facade of the Arab World Institute in Paris (see Figure 1).

As the weather patterns change, KSS are helpful because they can quickly adapt to the larger number of clear days and heat waves, providing better protection and comfort. In the context of climate resilience, KSS offer the following tools:

- Dynamic adaptation to environmental changes: KSS offer dynamic adjustment to variations in sunlight and temperature, mitigating the impact of extreme weather events and temperature fluctuations [6];
- Adaptation to shifting climate patterns: KSS optimize natural light levels while reducing reliance on artificial lighting and excessive air conditioning, thus adapting to changing climate patterns as proved by Ahmed et al. [7];

- Enhancement of building resilience: KSS protect against wind and debris during climate change-induced storms and extreme weather events, enhancing building resilience by design [8];
- Adaptive protection against extreme weather events: As climate change challenges urban environments, KSS offer adaptive solutions for creating sustainable and resiliently built environments, ensuring protection against extreme weather events [9].



(**a**) (**b**)

Figure 1. South facade of the Museum of the Arab World in Paris (arch. Jean Nouvel, 1987). (**a**) South facade view; (**b**) the detail of a mechanical diaphragm system (photo by the author).

Despite significant research interest, implementing KSS has been limited over the years due to the following selected challenges that must be explicitly outlined. Their complex mechanical components and advanced technology make them prone to malfunctions and operational issues, often requiring specialized repair services. Installing KSS involves advanced engineering and high-quality materials, leading to significantly higher construction costs than traditional shading solutions. Furthermore, their sophisticated design necessitates regular maintenance, which is costly due to the need for specialized technicians and high-tech component replacements. When activated to provide shade, KSS can obstruct views from windows, which may be undesirable for occupants who appreciate natural light and unobstructed outdoor views. Additionally, in temperate climates, KSS might reduce the beneficial greenhouse effect during winter by limiting the amount of direct sunlight that helps naturally warm the building. However, these obstacles should not discourage the further exploration and development of KSS because these systems have a high potential to improve the building's performance.

The author of the presented paper recently analyzed a vertical fin shading system in low winter solar altitudes in November 2023 [10]. While this system turned out to be quantitatively efficient in equalizing the level of scattered daylight in the room, it failed qualitatively by not mitigating glare, highlighting a critical issue in balancing light management and visual comfort. The next stage of the research is dedicated to horizontal fin KSS.

1.4. Horizontal Orientation of Fins

While KSS have evolved into diverse forms, including vertical and horizontal louvres or slats, previous research has demonstrated that horizontal fins are the most effective for south-facing facades, as proved by Alzoubi and Al-Zoubi [11]. This is because they can counteract high solar altitudes by efficiently blocking direct sunlight from entering the room, enhancing visual comfort and reducing solar heat gain. Horizontal shading systems are not only effective for south-facing facades but can also provide benefits in various climate zones. For example, in temperate regions, they can help control solar heat gain and glare during the summer months while allowing for passive solar heating in the winter.

2. State of the Art

The author examined the current knowledge and practices related to adaptive systems in general and KSS in particular. This review thoroughly summarizes the existing studies,

methods, technologies, and uses, along with the gaps, challenges, and opportunities for future research.

2.1. Review Method and Eligibility Criteria

Data for this review were sourced from international databases (WoS and Scopus, with the last search on 1 June 2024). The author looked for specific keywords in titles and abstracts. The search included terms like "kinetic facade", "adaptive facade", and "daylight", focusing on studies that simulated shading elements. References from previously reviewed papers were also considered.

The selection process involved multiple steps. Initially, the author (MB) reviewed titles and abstracts to identify studies focusing on topics related to "adaptive" and "kinetic" facades, which have been used in building engineering over the last two decades. Titles and abstracts from 2019 to 2023 were first examined, with duplicates removed. This process resulted in identifying 78 papers, of which 56 were chosen for further examination, ultimately including 28 papers in the literature review. Tables 1 and 2 present a comparison of various methods and conclusions from different research teams, and the primary review method was an online desk study without the use of automated tools.

2.2. Adaptive Facades

KSS are part of the broader "adaptive facades" domain, which includes systems that adjust based on external environmental conditions. Examples include variable transparency glass [12], dynamic wall insulation, liquid-filled panels, and systems using phase change materials [13]. The Adaptive Facade Network program COST TU 1403 (2016–2018) significantly advanced research in this area [14]. Notable reviews by AlDakheel [15] and Premier [16] highlight the prevalence of electrochromic systems and analyzed 51 case studies, respectively.

KSS offer a promising alternative for regulating daylight, using mechanical components like flaps and louvres powered by motors or actuators for translation, rotation, or folding movements. An early example is the kinetic system at the Museum of the Arab World in Paris (1988), which initially faced reliability issues and is now being restored. Mechanical motion challenges in KSS were explored in a recent review by the author in "Sustainability" [17].

2.3. Kinetic Shading Systems for Daylight Control

This chapter reviews studies on KSS, a subset of adaptive facades that use mechanical components to control daylight. The focus is on the control systems of KSS, which are crucial for optimizing performance and adaptability. Chan et al. (2015) analyzed a multi-sectional facade with light shelves, roller shades, and Venetian blinds, reporting significant energy savings and cooling load reductions [18]. Using ten operational steps, Lee et al. (2016) developed a heat transfer and daylight modelling approach for external shading devices [19]. Sheikh et al. (2019) proposed an adaptive biomimetic facade that reduced HVAC and lighting energy by 27–32%, utilizing the sun-path as a trigger for the KSS [20]. Grobman et al. (2019) found that horizontal fins improved performance by 6–34% by simulating KSS in seven discrete inclination states [6]. Damian et al. (2019) conducted a heat balance analysis on office buildings with KSS, demonstrating annual cooling load reductions of 36.9 to 42.8% using irradiance as a control trigger [21]. Luan et al. (2021) introduced a KSS inspired by origami, using Balancing Composite Motion Optimization activated by LEED point calculations [22]. Hosseini et al. (2021) reviewed various KSS, only evaluating them in discrete states [23]. Similarly, Sankaewthong et al. (2022) investigated a kinetic twisted facade with varying degrees of rotation [24]. Anzaniyan et al. (2022) concluded that bio-kinetic facades reduced electric lighting loads by about 48% without relying on external factor-based algorithms [25].

Mangkuto et al. analyzed horizontal louvre systems in tropical climates to meet the stringent requirements of LEED v4.1, using a discrete number of KSS states simulated over

a limited number of days [26]. Catto Luchino and Goia explored the application of horizontal louvres in double-skin facades, contributing to model-based control (MBC) strategies for optimizing the performance of louvre-based KSS in various architectural contexts [27]. Shen and Han evaluated two modular KSS—a conventional horizontal louvre shading system and a deformable triangular shading element—using 11 operational states and a surrogate model for daylighting and glare control [28]. Ożadowicz and Walczyk conducted an experimental study on a horizontal louvre system with integrated perovskite PV installations in Poland, optimizing configurations to maximize energy production using Somfy's "Maximum Power Point Tracking" algorithm [29]. De Bem et al. developed a low-cost responsive KSS prototype based on horizontal louvres, demonstrating its effectiveness at improving thermal and illuminance management triggered by solar altitude [30]. Kim et al. analyzed horizontal louvres made of electrochromic modules that adjust transmittance, functioning like standard louvres when open and mimicking a double-skin facade when closed, focusing on louvre count optimization with single-day simulations [31]. Norouziasas et al. evaluated the new ISO/DIS 52016-3 standard for adaptive façade simulations, finding that fixed horizontal shading outperformed dynamic Venetian blinds controlled by the ISO/DIS 52016-3 algorithm [32]. This standard was used by Norouziasas et al. and is not the basis for the presented research.

In 2024, the author of this study published an article on vertical KSS, validated through simulation and experimental testing. Three separate simulations per KSS state were conducted, and the final output was compiled by selecting the illuminance-dependent value at each timestep, proving quantitative efficiency but lacking in qualitative metrics [10]. Motion-based KSS, leveraging shape-memory and bi-stable flexible materials, have gained attention. Naeem et al. explored reducing cooling loads using shape-memory alloy (Nitinol) springs in shading louvres, with simulation angles based on experimental studies [33]. Vazquez and Duarte investigated bi-stable flexible materials actuated by shape-memory alloy (SMA) for control strategies in optimizing flap positions, providing innovative solutions for adaptive building envelopes [34]. Carlucci et al. advanced KSS studies by changing the paradigm to a gradual nature of KSS states, with algorithms combining sunlit fractions of each shading state [35] (see Table 1).

Table 1. Overview of key kinetic facade system studies detailing authors, publication years, the primary research focuses, and the control algorithm's description. This summary supports the analysis of current trends and challenges within the field, as outlined in the 'State of the Art' section.

Ref. No	Author:	Year	Main Focus	Control Algorithm (FCS)	Switching Schedule
[18]	Chan et al.	2015	• Multi-sectional facade combining solar protection and light-redirecting devices.	• Four scenarios. Effective illuminance control. • Set points at 1500, 2500, and 3000 lx. • Trigger: illuminance.	n.p.
[19]	Lee et al.	2016	• Computational model for heat transfer and daylight lighting for external shading devices.	• Shading operation scenario. • Ten operational steps: a shading device having an angle displacement of 0°, 20°, 40°, 60°, 80°, 100°, 120°, 140°, 160°, and 180°. • Trigger: solar heat gain, illuminance.	n.p.
[20]	Sheikh et al.	2019	• Adaptive biomimetic facade based on the redwood sorrel plant.	• Sensor feedback system. • Trigger: tracking the sun-path.	n.p.
[6]	Grobman et al.	2019	• Comparative analysis of daylighting performance in static and kinetic operation scenarios.	• Four scenarios, eight directions. • Seven fins inclination angles: −45°, −30°, −15°, 0°, 15°, 30°, 45°. • Trigger: UDI (named AUDI).	n.p.

Table 1. *Cont.*

Ref. No	Author:	Year	Main Focus	Control Algorithm (FCS)	Switching Schedule
[21]	Damian et al.	2019	• Heat balance analysis for a kinetic shading system in office buildings.	• Dynamic sun shading system. • Algorithm not provided. • Trigger: solar irradiance, outside temperature sensor.	n.p.
[22]	Luan et al.	2021	• Simulation study of kinetic shading systems inspired by origami.	• Algorithm: balancing composite motion optimization. • Trigger: ASE and sDA and the LEED v4 credits.	n.p.
[23]	Hosseini et al.	2021	• Review of kinetic systems and steering scenarios.	• Discrete states of the KSS only • Eval.: ASE and sDA and eUDI	n.p.
[24]	Sankaewthong et al.	2022	• Experimental study of a newly designed kinetic twisted facade.	• KSS rotating: 20°, 50°, 80° and 100°. • KSS twisting: 20°, 50°, 80° and 100°. • Discrete states of the KSS only. • Eval.: sDA (%) ASE (%).	n.p.
[25]	Anzaniyan et al.	2022	• Bio-kinetic facade integrating architecture, biomimicry, and occupant comfort.	• Experimental setup based on the geometry of *Lupinus succulentus* • No algorithm was given. • Three scenarios: static, rotated 50° in the warm months, rotated 20° in the cold months.	n.p.
[26]	Mangkuto et al.	2022	• Analysis of horizontal louvre systems in tropical climates to meet LEED v 4.1 requirements. • Determination of optimal slat configurations for balancing daylighting and energy efficiency.	• Discrete states of the KSS only. • Discrete days of the year only. • Trigger: sorting all possible combinations and finding the one with $sDA_{300/50\%}$ and $ASE_{1000,250}$ that have the least distance to (100%, 0%) in each scenario.	n.p.
[27]	Catto Luchino and Goia	2023	• Exploration of horizontal louvre systems in double-skin facades. • Development of control strategies for optimizing louvre-based kinetic facade systems in different architectural contexts.	• Model-based control (MBC) is to run parametric simulations over the entire domain of possibilities for a given timestep. • Trigger: illuminance, CO_2 concentration, temperature. • MBC scheme provided.	yes, 7 days
[28]	Shen and Han	2022	• Evaluation of modular kinetic facade systems, including conventional and deformable louvre systems, • Assessment of modular control strategies.	• Eleven operational steps of KSS • Integer programming equation with sky vector as an input at given time steps to obtain optimal KSS state. • Trigger: sky vector. • The surrogate model is used as an approximation.	yes, 31 days
[29]	Ożadowicz and Walczyk	2023	• Optimization of louvre configurations to maximize energy production yield while effectively managing thermal and illuminance levels.	• Maximum Power Point Tracking (MPPT) algorithm. • Animeo IB+ control system. • Trigger: illuminance	n.p.
[30]	de Bem et al.	2024	• Presentation of a low-cost responsive shading system prototype based on horizontal louvres. • Effectiveness of responsive louvre-based kinetic facade systems in improving thermal and illuminance management.	• Slats' rotation angle: 0% shading for maximum sunlight penetration, 50% for a striped pattern, and 100% for full coverage—timestep 10 min. • Trigger: solar altitude.	n.p.
[31]	Kim et al.	2022	• Exploration of electrochromic louvres for meeting daylight criteria and energy performance standards.	• Discrete states of the KSS only. • One day of the year only: 30th March. • Variable number of horizontal louvers.	n.p.

Table 1. *Cont.*

Ref. No	Author:	Year	Main Focus	Control Algorithm (FCS)	Switching Schedule
[32]	Norouziasas et al.	2023	• Investigation of particularly dynamic shading systems in meeting energy performance standards.	• Control strategies recommended by ISO 52016-3. • Flowcharts of automated control strategies were provided.	yes, 356 days
[10]	Brzezicki	2024	• Daylight Comfort Performance of a Vertical Fin Shading System. • Construction of a reduced-scale mock-up for real weather measurements.	• KSS control strategy according to internal illuminance. • Trigger: internal illuminance	n.p.
[33]	Naeem et al.	2024	• Explored reduction of cooling loads using shape-memory alloy (Nitinol) springs in shading louvres. • Integration of shape-memory alloy springs with building automation systems.	• KSS angles depend on the angles proposed by the experimental study. • Four days of the year only: 21st July, September, August, and October.	n.p.
[34]	Vazquez and Duarte	2022	• Conducted experimental research on bi-stable flexible materials actuated by shape-memory alloy (SMA). • Development of control strategies for optimizing flap positions in bi-stable kinetic facade systems.	• The control mechanism allows only three different configurations for the bi-stable screen, 'open', 'closed', and '50% open/closed'.	n.p.
[35]	Carlucci et al.		• Development and validation of a tool based on Python and Energy-Plus that can consider the continuous nature (gradual states) of the energy simulation. • Continuous shading adjustments.	• The algorithm combines the sunlit fractions of each shading state (combined inputs) and uses this combined file as an external shading file of the simulation. • Workflow conceptualization diagram.	yes, 365 days

n.p.—not presented.

Table 2. Geometries' characteristics per material. This table includes all relevant optical properties and their corresponding materials, as detailed in the paragraph above.

	Vertical Surfaces	Work Plane	Standard Window	Kinetic Fins	Floor
Material	White paint	Dark gray (RAL 7000)	Transparent glass	Gray metal	Light gray
Reflectance	0.80	0.23	0.19	0.5	0.65
Transmittance	0	0	0.64 [1]	0	0

[1] Parameter of a double layer of 3 mm Pilkington Standard Glass.

3. Objectives, Methodologies, and Innovations in Research

This paper introduces several key innovations in the field of KSS, enhancing the adaptability and efficiency of building facades to improve visual comfort and energy performance in response to diverse climatic conditions:

- Bi-Sectional KSS: The paper introduces a novel bi-sectional KSS design that allows independent control of shading fins. This feature provides precise daylight management and reduces glare, effectively adapting to different climate conditions. Previous research on multi-sectional facades combining solar protection and light-redirecting devices mentions control strategies but does not explore algorithmic innovations for KSS [18].

- Dual Approach Methodology: This combines both simulation and experimental analyses. The paper offers a comprehensive evaluation of the KSS' performance, enhancing the reliability and applicability of the findings. The experimental setup achieves a rapid temporal resolution significantly faster than existing systems, e.g., [29,33,34], marking a substantial advancement in system responsiveness and control precision. By integrating new methods and data, this study addresses gaps in current research and lays the groundwork for future exploration in adaptive facade technologies.
- Bespoke Mock-up for Experiment: The prototype was constructed at a 1:20 scale, using precision laser cutting techniques. The structure comprises particle board and 3 mm-foamed PVC—materials selected for their durability and ease of fabrication.
- Python Script: This was developed for this project and offers a high degree of versatility, enabling customization of threshold illuminance levels, hysteresis, and motor step control. This flexibility allows it to address a wide range of daylight management scenarios, making it an innovation in its own right. Beyond its application in the current test stand, the script can be adapted for use in other daylight management installations.
- Integration of Mock-up and Software: Two stepper motors, Raspberry Pi 3 (manufact. Raspberry Pi Foundation, Cambridge, UK) and software Python v. 3.11 script, are set up for real-time data collection and processing with a temporal resolution of 2 s. This integration presents a novel approach to data collection in daylight studies, as it allows for the precise monitoring of both groups of fins. With 43,200 illuminance data points collected daily, the system can generate significant data.
- Custom Metrics for Performance Evaluation: The development of custom metrics such as $UDI_{300–3000}$, DA_{500} uniformity, and operational constraints of the KSS provides a more nuanced understanding of daylight performance across different climates.
- Facade Closure Scheme (FCS): Implementing an illuminance-dependent algorithm to adjust shading configurations dynamically is a significant advancement, offering a precise method to maintain visual comfort within buildings.
- KSS Switching Schedules (KSS): Comprehensive diagrams depicting the KSS's operational states for every sun hour throughout the year. These KSS demonstrate significant variations, effectively illustrating how the system adapts to the distinct sun paths and cloud covers specific to each location. Including these detailed FSS diagrams is a rarity in the existing literature, further emphasizing the innovative nature of this research.
- Angle heat maps: using heat maps to illustrate various angles of fin inclination with colour coding is a method not previously documented in the existing literature, establishing it as an original contribution.
- Various climatic conditions: testing the performance of KSS across different climatic conditions, highlighting its adaptability. The previous paper focused more on fixed facade configurations than dynamic adaptability [18].

3.1. Bi-Sectional KSS Design Description

The proposed bi-sectional KSS was designed to shade a 4.0 × 4.0 m southern facade in an office room with 4.0 × 8.0 m plan dimensions. The bi-sectional KSS system consists of six kinetic fins that are rotated around an eccentric axis located along the longer edge of the fins. The fins are 66 cm wide and 380 cm long. The system is mounted in a supporting frame with a depth equal to the width of the fins. The exact geometry of the system is presented in Figure 2.

Uniquely, the six fins are divided into two groups of three, with fin numbers 1–3 and numbers 4–6 capable of being closed independently, based on a schedule derived from measurements of internal illuminance levels. This distinctive feature is hoped to precisely mitigate excessive illuminance near the glazing while maximizing daylight penetration into the deeper areas of the room.

The design of the bi-sectional KSS represents a novel approach to facade technology, offering unparalleled control over daylight comfort and energy efficiency. Fins numbered 1–3 in the system will be further referred to as 'lower fins', while fins numbered 4–6 will

be referred to as 'upper fins'. The angle of inclination for the lower fins will be denoted as 'α_{dn}', and for the upper fins, it will be denoted as 'α_{up}'.

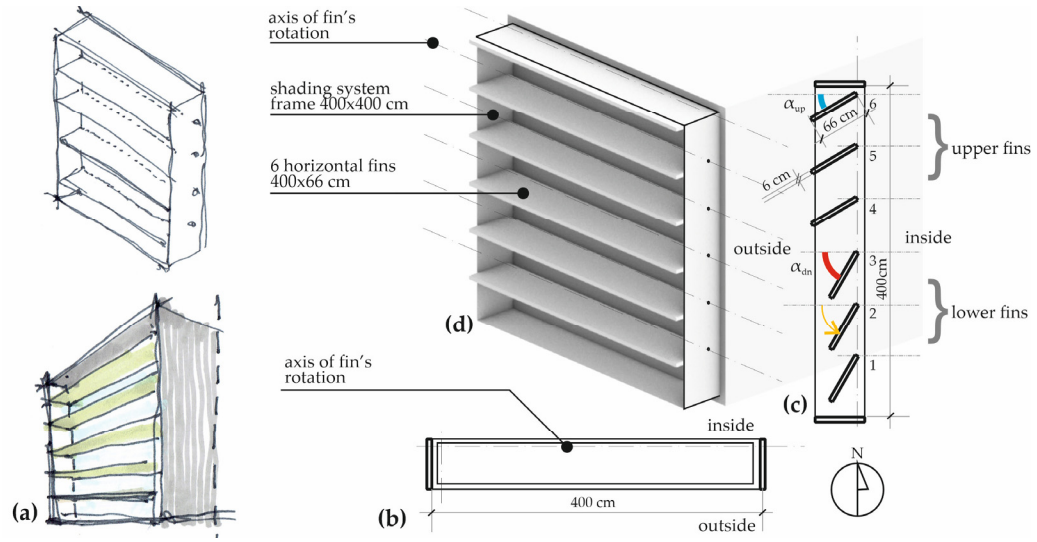


Figure 2. Bi-sectional KSS proposal: (**a**) conceptual sketches, dimensions of the proposed KSS (**b**) horizontal section; (**c**) vertical section; (**d**) axonometric view. The angles α_{up} (marked in blue) and α_{dn} (marked in red) are the horizontal fin rotation angles for the upper and lower fins, respectively. The gray arrow indicates the direction of rotation.

3.2. Facade Closure Scheme

The facade closure scheme (FCS) plays a pivotal role in controlling the performance of the bi-sectional KSS; this is an algorithm according to which the kinetic behavior of the facade is managed. This study determines the FCS based on the office room's illuminance levels. A single sensor, designated as sensor 'A', is strategically positioned at a distance of 1.5 m from the facade and 0.85 m above the floor, corresponding to the typical work plane height. The sensor's location is consistent in both the simulation and the physical experiment, where it is referred to as sensor 'A_1'. Sensor 'A' was selected for its location based on initial simulations and experiments conducted with a different KSS geometry [10], which identified this position as critical for achieving optimal visual comfort due to elevated illuminance levels. Initial measurements in the preparatory stage consistently showed illuminance above 300 lx at the back of the Test Room, addressing concerns about reduced lighting away from the facade.

The control algorithm for the Facade Control System (FCS) is designed to maintain visual comfort within the parameters outlined by the LEED v.4 standards, using an upper threshold of 3000 lux (abbreviated as "lx") as the "trigger value". The FCS operates based on illuminance readings from sensor 'A' and adjusts the facade fins accordingly:

- Initial State (Open Configuration): When the illuminance at sensor 'A' is below 3000 lx, both the upper and lower groups of facade fins remain in the open position, perpendicular to the facade (angle = 0° relative to the facade's normal), denoted as the KSS configuration 'open'.
- Lower Fin Adjustment (Down-Closed Configuration): When the illuminance at sensor 'A' exceeds the 3000 lx threshold, and the lower fins automatically rotate to reduce the illuminance levels at sensor 'A'. In the simulation, this configuration is termed 'down-closed', where the lower fins are adjusted to an angle of 60° relative to the facade's normal. In the experiment, the lower fins gradually rotate in 1° increments until the angle of 60° is reached.
- Upper Fin Adjustment (All-Closed Configuration): If the illuminance level at sensor 'A' continues to exceed 3000 lx even after the lower fins have been adjusted, the upper fins are rotated to decrease the illuminance further. In simulation, this configuration

is called 'all-closed', where both the upper and lower fins are set at an angle of 60° relative to the facade's normal. In the experiment, the upper fins gradually rotate in 1° increments until the angle of 60° is reached.

Operational Constraints: In simulation, the fins can only be positioned at discrete angles of either 0° or 60° relative to the facade's normal. The FCS does not typically specify full closure of the fins to allow some degree of natural light penetration, however, full closure may be utilized for facade protection during extreme climate conditions. The algorithm thus provides a stepwise adjustment of the facade elements to optimize internal lighting conditions while adhering to specified visual comfort limits. For a visual representation of these configurations, refer to Figure 3.

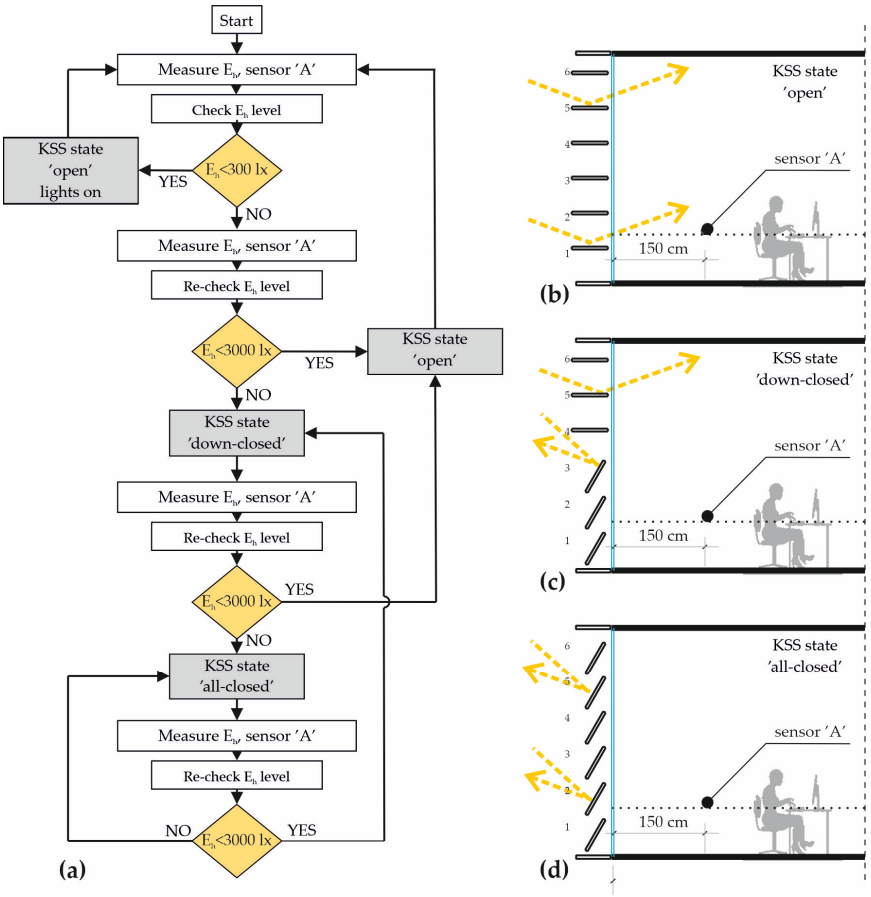


Figure 3. Facade Closure Scheme (FCS): (**a**) flowchart for one iteration. The FCS uses sensor 'A' to control the KSS. Fins remain open if E_h is below 3000 lx (KSS 'open'). Lower fins close if E_h exceeds 3000 lx (KSS 'down-closed'), and upper fins close if it rises further (KSS 'all-closed'). If E_h drops below 300 lx, artificial lights are activated. In the simulation, the FCS is simplified, with fins restricted to discrete positions of either 0° or 60°, whereas in the experiment, intermediate positions are allowed, (**b**) the section of the Test Room showing KSS state 'open'; (**c**) the section of the Test Room showing KSS state 'down-closed'; (**d**) the section of the Test Room showing KSS state 'all-closed'. The yellow dashed arrow indicates the direction of the rays of light.

The FCS was simplified for simulations because the daylight simulation software operates in 1-h increments, therefore, there is insufficient temporal resolution (e.g., the number of sun-hours in Wroclaw in the winter is only eight). Analyzing all the intermediate angles would significantly complicate the algorithm and increase the computational load. Simplifying the angles to only 0° and 60° reduces the complexity, making the simulation more efficient and faster. It also minimizes potential errors that could arise from handling a wide range of angles, ensuring more reliable and consistent outcomes in the daylight analysis.

In the experiment, illuminance levels are measured every 2 s to ensure the precise monitoring of light conditions. The fins are rotated gradually, starting with the lower fins followed by the upper fins at a tilt angle of 1° per adjustment. This results in a total of 120 positions for the fins, allowing for fine-tuned control over the lighting environment. This experimental setup provides a detailed assessment of how the FCS responds to changes in illuminance, enhancing the understanding of its performance under varying conditions.

In this study, the 'trigger value' is the illuminance level E_h measured by sensor 'A'. Still, other environmental parameters, such as global horizontal irradiance (GHI) measured outside the Test Room, may also be used. However, the illuminance measured inside is already altered by the horizontal fins of the bi-sectional KSS. At the same time, GHI only depends on solar irradiance and solar position.

The control strategy for the KSS in the simulation is limited to three intermediate states. The full kinetic cycle, from the 'open' state in the morning to the 'open' state in the evening, requires four state changes, assuming a perfectly parabolic irradiance curve. Introducing a higher number of intermediate states (e.g., fins rotated at 30°) would require eight state changes at 1-h intervals, which could only be accommodated on the longest clear day of the year when illuminance values above 3000 lx are recorded for eight hours. This approach would compromise the control strategy on days with shorter daylight duration by necessitating either fewer state changes or a more condensed and less accurate adjustment schedule.

3.3. Applied Research Methods

The author conducted two types of analysis on the proposed bi-sectional KSS:

- Phase One involved annual simulations of Useful Daylight Illuminance ($UDI_{300–3000}$), Daylight Autonomy (DA_{500}), and glare using standardized weather data from the EnergyPlus database for specified locations. This phase examined three geometrical configurations of the KSS: open, down-closed, and fully closed, operating according to the Facade Closure Scheme (FCS).
- Phase Two consisted of experimental illuminance measurements conducted on selected June and July 2024 days in Wroclaw, Poland (latitude 51°). These measurements were performed using a south-facing, reduced-scale 1:20 mock-up of the bi-sectional KSS facade mounted on a testbed specifically designed for daylight measurement. Figure 4 illustrates the schematic diagram of the methodology.

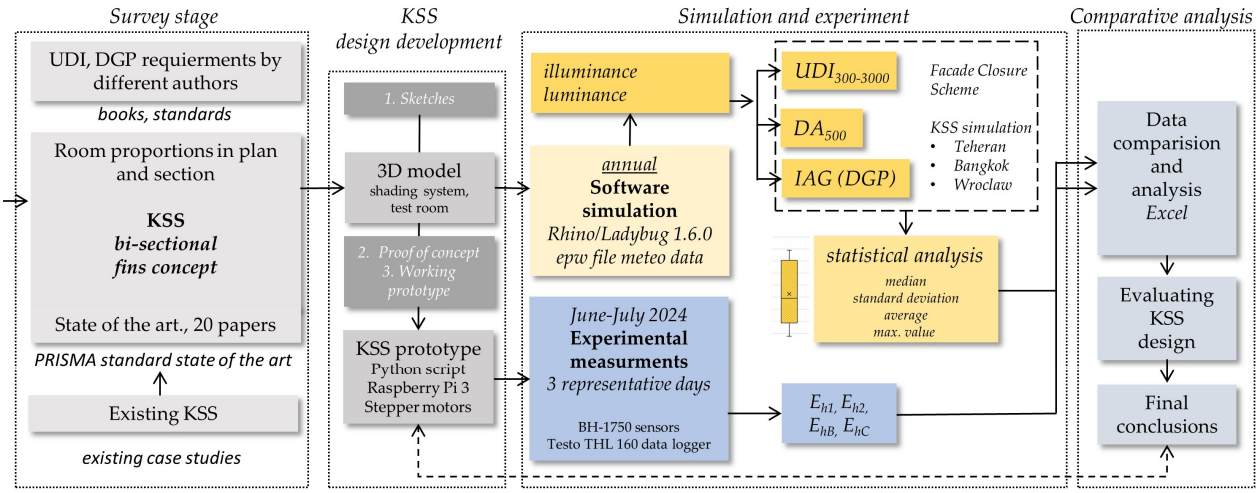


Figure 4. Schematic diagram of the methodology for simulation in various locations and experimental illuminance measurements of the KSS facade in Wroclaw, Poland. 'UDI' denotes Useful Daylight Illuminance, 'DA' denotes Daylight Autonomy, 'DGP' denotes Daylight Glare Probability, and 'E_x' denotes horizontal illuminance for various sensors.

The methods section is divided into two parts and will be presented in the corresponding chapters. The first part details the simulation methodology, focusing on the computational analysis conducted to assess the performance of the bi-sectional KSS. The second part outlines the experimental design, describing the setup and procedures used to validate the simulation results and evaluate the shading system's practical feasibility in real-world conditions.

The combined approach of simulation and experimentation provides a comprehensive evaluation of the bi-sectional KSS's effectiveness in enhancing daylight comfort and climate resilience across diverse climatic contexts (see Figure 4).

3.4. Research Objectives

The objectives focus on evaluating and demonstrating the bi-sectional KSS's capabilities in enhancing daylight comfort and climate resilience while emphasizing its applicability in sustainable building design. The main goals are as follows:

- Demonstrate Effectiveness: Show the effectiveness of the horizontal bi-sectional kinetic shading system (KSS) in improving visual comfort across diverse climate zones, including hot and arid, temperate, and hot and humid regions.
- Dual Approach Evaluation: Use a dual approach combining simulation and experimental analyses to evaluate the system's ability to optimize daylight distribution, reduce glare, and maintain comfortable luminance levels within buildings.
- Simulation and Experimentation: Conduct detailed simulations and experimental analyses using scaled models and real-world measurements to empirically validate the system's performance, ensuring the results are reliable and applicable to practical scenarios.
- Provide Robust Evidence: Offer robust evidence supporting the effectiveness of bi-sectional KSS in adapting to varying climatic conditions and advancing the understanding of sustainable building design practices.
- Guide Future Designs: Demonstrate the effectiveness of the KSS in inspiring the integration of shading technologies that enhance sustainability and comfort in architecture.
- Promote Resilient Design: Stress the need for adaptive design strategies to develop robust buildings against varying and changing climate conditions.

4. Simulation

Daylight simulation was conducted using the Climate-Based Daylight Modelling (CBDM) method, a standard practice in sustainable architectural design.

4.1. Simulation Method

The author utilized Rhino, version 7, to model the virtual office Test Room and the proposed KSS. Daylight simulations were conducted using the Ladybug/Honeybee 1.6.0 plugin with the Radiance daylight simulation engine. This tool's reliability has been confirmed by numerous prior studies, such as those by Reinhart and Walkenhorst [36], Ng et al. [37], and Yoon et al. [38]. In a 2020 publication in the journal Solar Energy, Kharvari validated the accuracy of the Honeybee/Ladybug plugin for Rhino through experimental validation of the Radiance computational engine embedded in Ladybug, using "grid analyses under an overcast sky with a certain illuminance level" [39]. Kharvari's findings showed that the average difference between calculated and measured illuminance levels for all points was 9%, and the average room illuminance level was 2%. These results indicate that Radiance accurately estimates the overall illuminance level on the analysis grid. Kharvari concluded, "[. . .] Radiance is still the most powerful and accurate tool for predicting illuminance levels in buildings" [39]. Furthermore, Reinhart and Andersen demonstrated that translucent materials "can be modelled in Radiance with an even higher accuracy than was demonstrated earlier [. . .]" [40].

In computer simulation using the Radiance/Honeybee plugin, variable geometry models are not possible, e.g., it is impossible to automatically model a fin at a different angle for different sun-hours. This obstacle is addressed using a method proposed by

Ch. Reinhart in the 'Daylighting Handbook II' [41]. The method involves calculating illuminance levels for discrete states of the KSS (e.g., open, down-closed, all closed) and then using a code or formula to determine the correct values for each sun-hour of the year based on the 'trigger value'. A similar approach was suggested by Do and Chan in 2018 [42] and is analyzed in the paper by Carlucci et al. [35].

Following the above, the so-called *discrete state illumination method* (DSIM) was employed to simulate the operation of bi-sectional KSS. This approach simulates illuminance values for each discrete state of the bi-sectional KSS for an entire year—approx. 4400 sun-h (the exact number differs regarding location). The results are then integrated by a script that assigns a specific facade state and corresponding illuminance values to every sun-hour of the year based on predefined criteria. In the presented research, the criterion is the internal horizontal illuminance level E_h at the virtual sensor 'A'. This comprehensive method allows for an in-depth analysis of how different facade configurations impact daylight performance throughout the year.

The Ladybug/Honeybee 1.6.0 plugin uses the Radiance daylight simulation engine and the 'HB-Annulal-Daylight' component to allow daylight simulations at a 1-h timestep. Post-processing methods used to calculate metrics like $UDI_{300–3000}$ and DA_{500} rely on a 1-h timestep to ensure the illuminance values correctly align with the occupancy schedule [43].

The model was calibrated by calculating R^2, CV (RMSE), providing the calibration and error charts, however, obtaining more data over a longer measurement period will further enhance the robustness of this process (see Appendix A).

4.2. Simulation Setup for $UDI_{300–3000}$, DA_{500} and DGP

The simulation focused on a standard office Test Room measuring 4 × 8 m with a height of 4 m, oriented directly southward to represent typical office building configurations. The Test Room is side-lit by a large glazing that spans from the floor to the ceiling. The bi-sectional KSS is mounted outside. All the optical parameters of the materials are provided in Table 2. The illuminance levels are calculated for a work plane located at a height of 0.85 m above the floor, using a grid of 0.5 × 0.5 m with 128 sensors. A single virtual sensor, labelled 'A', positioned centrally 1.5 m from the glazing, was selected to provide illuminance values that served as the 'trigger value' for switching the states of the bi-sectional KSS, as shown in Figure 5.

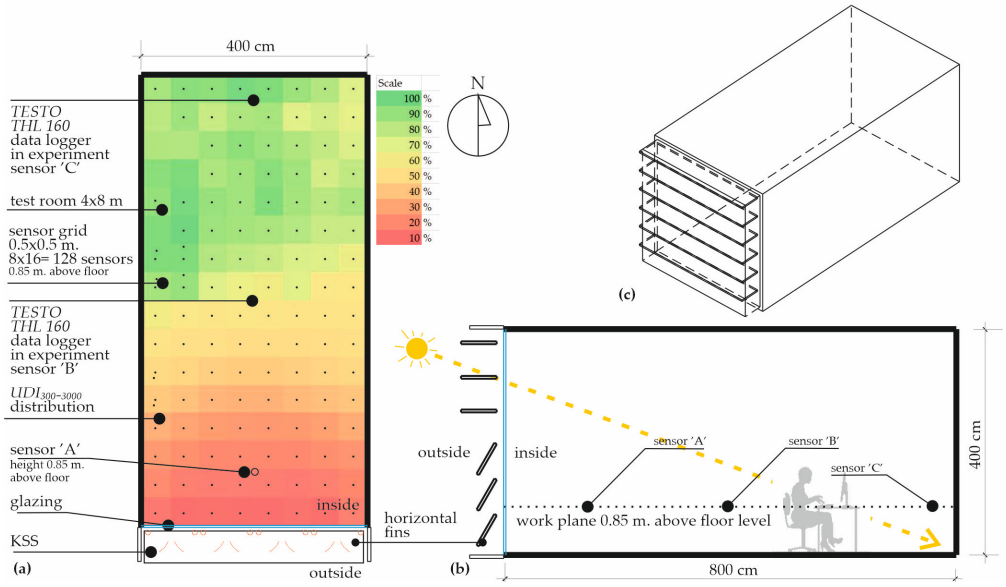


Figure 5. Simulation setup of the Test Room: (**a**) plan showing the location of the shading fins and virtual sensors, and the location of sensors 'A', 'B', and 'C'; (**b**) section showing the location of the shading fins; (**c**) an axonometric view showing the Test Room with the shading system mounted.

The simulation was run for every day of the year to ease the presentation of switching schedules for the bi-sectional KSS. While it is customary to analyze office rooms only for weekdays, extending the analysis to include all days of the year offers a comprehensive understanding of the system's performance across different seasonal variations and weather conditions. Since different cultures and calendars may have different conventions for the start of the year, analyzing switching schedules for every day of the year ensures a comprehensive assessment of the system's performance across all possible scenarios.

4.3. Climate and Location Variants

Simulation studies assessed the bi-sectional KSS's performance in three distinct climate conditions: (i) Wrocław, Poland (51.1° N), (ii) Tehran, Iran (35.7° N), and (iii) Bangkok, Thailand (13.8° N). The cities are always ordered according to the geographical location (from the northernmost to the southernmost). Climate data for each location were obtained from *.epw standard weather files from the EnergyPlus library and fed into the Honeybee Radiance plugin within the Grasshopper/Rhino software version 1.6.0 [44].

The selected climates were intentionally diverse, covering a range of factors relevant to daylight analysis. Specifically, the diversity across the three climate zones is characterized by (i) variations in latitude, leading to distinct sun paths and solar altitude angles; (ii) differences in cloud coverage, with Tehran experiencing the clearest skies; (iii) variations in GHI, with Tehran exhibiting the highest values and Wroclaw the lowest; (iv) discrepancies in the number of clear days experienced in each climate zone. These factors collectively contribute to a comprehensive understanding of the impact of climate on daylight performance across different geographic regions.

4.4. Performance Indicators

The simulation presented in this study is based on standard indicators used for daylight assessment, and custom indicators determined by the author that explicitly represent the characteristics of the presented bi-sectional KSS system.

4.4.1. Standard Indicators

The analysis uses quantitative metrics designed around illuminance levels. The primary metric used is Useful Daylight Illuminance (UDI), which quantifies the percentage of sun-hours throughout the year during which horizontal illuminance (E_h) values fall within the range of 300 to 3000 lx. This metric is commonly denoted as $UDI_{300–3000}$. It was first defined by Nabil and Mardaljevic in 2005 as a metric that "determines the percentage of the time that the interior daylight illuminance in a room falls within a user-defined range" [45]. Boubekri and Lee attested to the relevance of this metric. The 300 to 3000 lx range selection is based on their paper in [46] and the LEED v 4.0 standard, which requires that "illuminance levels will be between 300 lx and 3000 lx for 9 AM and 3 PM" [4]. A daylight autonomy study was also conducted to verify the sufficiency of daylight levels deep in the back of the room. This threshold was selected since 500 lx is the set point illuminance for offices. DA_{500} was calculated based on the illuminance values in the Test Room.

A qualitative study was performed using daylight glare probability (DGP). DGP was defined for the first time in 2006 in a paper published by Wienold and Christoffersen in 2006 [47]. This approach enables a direct comparison of glare potential across different climatic conditions, ensuring that any variations in the DGP are due to differences in climate rather than changes in analysis parameters. Imageless Annual Glare diagrams provided a comprehensive overview of glare potential throughout various seasons of the year.

According to Wienold and Christoffersen, with DGP above 35% (<2000 lx), the glare is rated as "Perceptible", while with DGP above 45% (>6000 lx/> 4500 lx) the glare is "Intolerable". The formula for calculating the Daylight Glare Probability (DGP) is well documented in various sources [10,47], so it is not repeated here each time DGP is calculated.

4.4.2. Custom Indicators

In evaluating the effectiveness of bi-sectional KSS within office spaces, it is essential to use multiple performance metrics. This study expands beyond the basic assessment of UDI and DGP. To assess the uniformity of daylight distribution throughout the office space, the study introduces a measure denoted as UDI uniformity—U_{UDI}. This is calculated using the following formula (1):

$$U_{UDI} = \frac{UDI_{min}}{\overline{UDI}} \quad (1)$$

is used to assess the uniformity of illuminance distribution across the office space. Similarly, the uniformity of DA_{500} is calculated in the same way. Other statistical metrics are derived from the final $UDI_{300–3000}$ and DA_{500} distribution across the room plans. The list of metrics is provided below in Table 3.

Table 3. Summary of key performance statistical metrics.

	Metric	Unit	Description
UDI area specific	U_{UDI}	n.a.	UDI uniformity for final $UDI_{300–3000}$ distribution
	σ_{UDI}	n.a.	Standard deviation σ for final $UDI_{300–3000}$ distribution
	$\widetilde{m}_{UDI}$	n.a.	Median for final $UDI_{300–3000}$ distribution
	UDI_{max}	[%]	The maximal UDI for the final $UDI_{300–3000}$ distribution
	$\overline{UDI}$	[%]	Average UDI for final $UDI_{300–3000}$ distribution
DA area specific	U_{DA}	n.a.	DA uniformity for the final DA_{500} distribution
	σ_{DA}	n.a.	Standard deviation σ for final DA_{500} distribution
	$\widetilde{m}_{DA}$	n.a.	Median for final DA_{500} distribution
	DA_{max}	[%]	The maximal DA for the final DA_{500} distribution
	$\overline{DA}$	[%]	Average DA for final DA_{500} distribution

4.5. Simulation Results

4.5.1. Quantitative Study

For comparison, the author simulated three variants: (i) the Test Room without any shading device, (ii) the bi-sectional KSS in the 'open' state (α_{dn} and $\alpha_{up} = 0°$), and compared it with the simulation of (iii) the bi-sectional KSS in full operation mode, following the FCS described above. Simulations were conducted for three climate zones, and the results were statistically analyzed and presented as box plots and histograms.

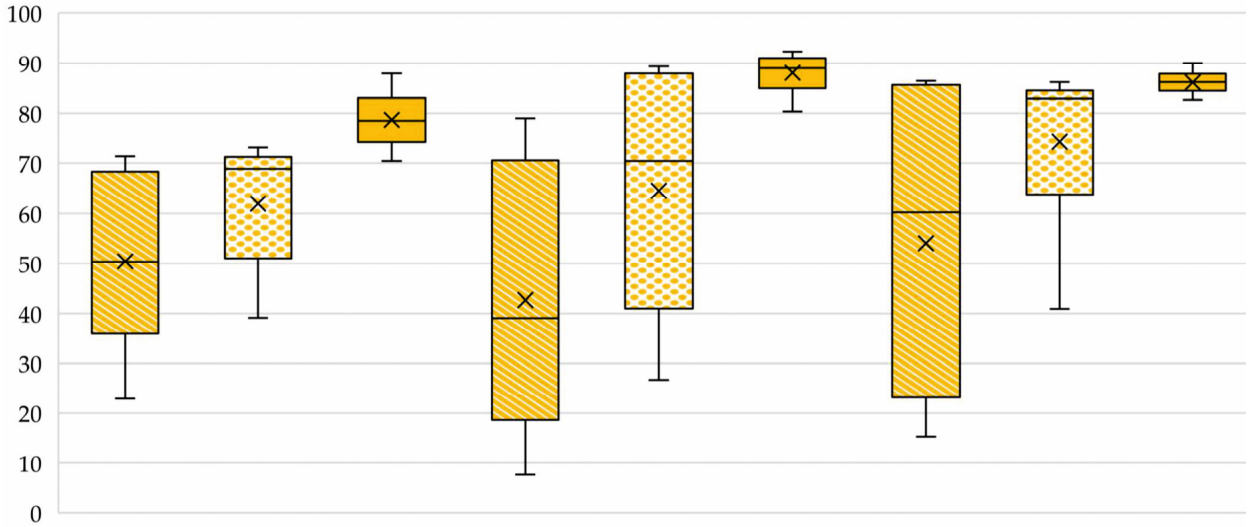
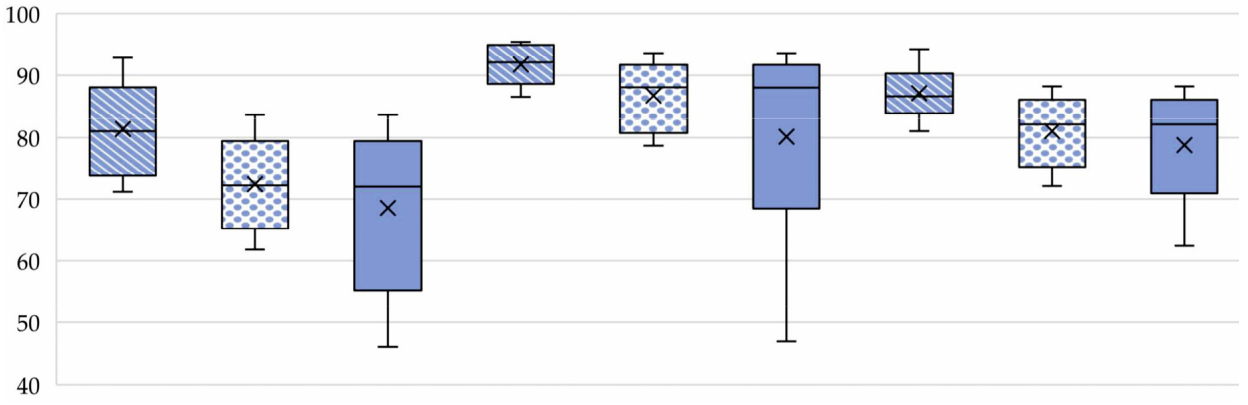
- $UDI_{300–3000}$

Without any shading device, the $UDI_{300–3000}$ shows high variability. The IQR ranges from 20 to 70 in Wrocław, 7 to 80 in Tehran, and 15 to 85 in Bangkok, indicating greater variation in values due to significant over-illumination near the glazing. The median values are relatively low at 50.39%, 39.10%, and 60.27%, respectively. These findings align with comparative studies by the author on GHI values for each location. Tehran experienced the highest GHI values and number of clear days, resulting in significantly diverse values of $UDI_{300–3000}$ recorded. Bangkok also recorded high GHI values but with fewer clear days. Wrocław, with the lowest GHI values and even fewer clear days, exhibited the lowest variability in $UDI_{300–3000}$ values.

Installing the KSS system in the 'open' state visibly reduces variability, shifting the values toward higher levels, with medians of 68.93%, 70.40%, and 82.88%, respectively. The application of the FCS system further enhances performance, characterized by low variability, the highest $UDI_{300–3000}$ values, and elevated medians. The most significant improvement over the 'no-shading' scenario was observed in Bangkok, though all analyzed cities exhibit high uniformity, low standard deviation, and elevated average $UDI_{300–3000}$ values. Specifically, uniformity U_{UDI} improved to 0.89 in Wrocław, 0.96 in Bangkok, and

0.94 in Tehran. In addition to the improved distribution of $UDI_{300–3000}$ values, other metrics also show marked enhancement in quantitative visual comfort, as detailed in Table 4. These findings suggest that the bi-sectional KSS system significantly improves daylight distribution within the room, with all quantitative metrics reflecting better performance.

Table 4. Statistical analysis of quantitative visual comfort metrics: $UDI_{300–3000}$ and DA_{500}. Box plot graphs illustrate the distribution of $UDI_{300–3000}$ and DA_{500} values. Additionally, average, median, and standard deviation values are provided to evaluate visual comfort. The data compare three scenarios: no shading, open static fins, and the Facade Closure Scheme across all locations.

	Wrocław			**Tehran**			**Bangkok**		
	no shading	open fins	FCS	no shading	open fins	FCS	no shading	open fins	FCS
$UDI_{300–3000}$ [%]									
U_{UDI}	0.45	0.63	0.90	0.18	0.41	0.91	0.28	0.55	0.96
σ_{UDI}	16.56	11.20	4.94	24.98	22.59	3.25	28.25	13.25	1.83
$\widetilde{m}_{UDI}$	50.39	68.93	78.51	39.10	70.40	88.96	60.27	82.88	86.22
UDI_{max}	71.36	73.12	87.90	78.96	89.36	92.30	86.44	86.22	90.03
$\overline{UDI}$	50.42	61.99	78.68	42.72	64.60	88.02	54.14	74.19	86.11
DA_{500} [%]									
U_{DA}	0.87	0.85	0.67	0.94	0.91	0.59	0.93	0.89	0.79
σ_{DA}	7.31	7.30	12.26	3.05	5.15	14.67	3.81	5.33	8.54
$\widetilde{m}_{DA}$	81.04	72.23	72.01	92.05	88.02	87.98	86.60	82.13	82.13
DA_{max}	92.83	83.60	83.60	95.41	93.56	93.56	94.20	88.17	88.17
$\overline{DA}$	81.39	72.43	68.53	91.72	86.70	80.12	87.11	81.04	78.77

- DA_{500}

Given that the set point illuminance in offices is typically 500 lx, DA for the 500 lx threshold was calculated to assess the impact of the KSS system on DA_{500} distribution. The key finding from this analysis is that the operation of KSS in FCS mode significantly reduces DA_{500} in the back of the room by approximately 12.5% compared to the KSS in the 'open' state and by 30.5% compared to the KSS performing FCS. Box plots illustrate increasing variability, with whiskers extending to below 50%. Additionally, histograms reveal a shift in DA_{500} values toward lower levels with decreased occurrence, which contrasts with the trends observed in the $UDI_{300–3000}$ histograms (see Figure 6).

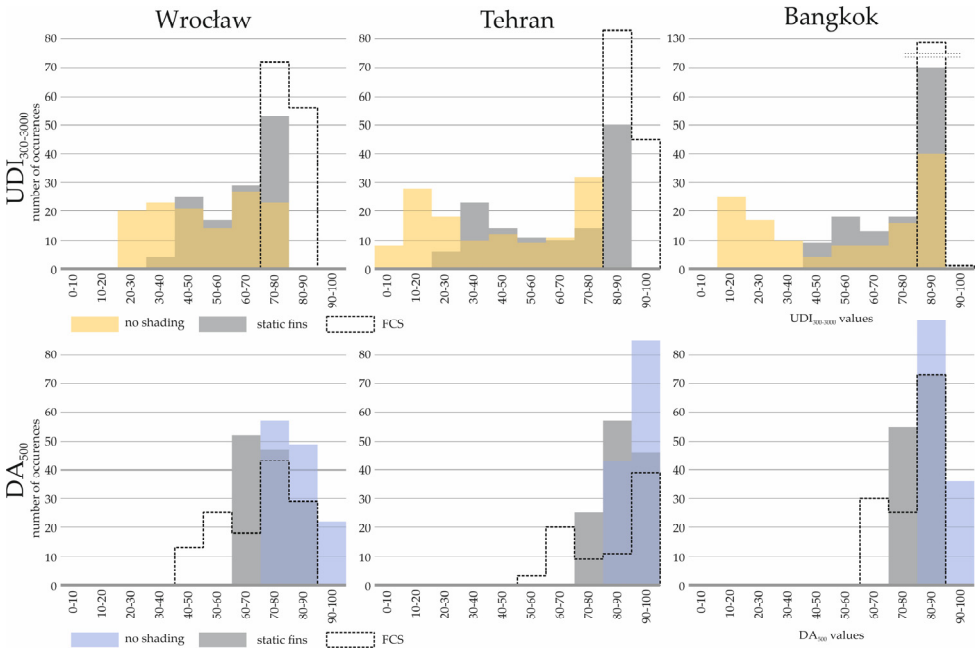


Figure 6. Histograms illustrating the distribution of $UDI_{300–3000}$ and DA_{500} values across three cities. The charts provide a comparative analysis of daylight performance metrics, highlighting variations in natural light availability depending on the adopted shading scenario.

Closing the lower and upper fins effectively limits daylight penetration into the back of the room. However, it is essential to note that DA_{500} values remain above 50%, even under these conditions. In the worst-case scenario, with FCS in operation in Tehran, DA_{500} drops from 88% to 47% at the back of the room in the corner.

For a detailed view of the spatial distribution of quantitative visual comfort metrics, including $UDI_{300–3000}$ and DA_{500}, across the room plans, please refer to the Supplementary Materials (see Supplementary_Data_S1.xlsx).

- KSS switching schedules

Based on E_h's calculated illuminance values, the bi-sectional KSS was 'launched' in full operation mode according to the FCS. An additional simulation outcome is the switching schedules (FSS), which are diagrams showing the KSS's state during every sun hour of the year. These FSS differ significantly between Wrocław, Tehran, and Bangkok, highlighting the differences in each location's varying sun paths and cloud cover.

The analysis of the bi-sectional KSS's operation across Wroclaw, Tehran, and Bangkok reveals distinct operation patterns adapted to each location's specific climatic conditions (see Table 5). In Wroclaw, the bi-sectional KSS is open (state: open) 23.81% of the time, suggesting that the natural light levels in Wroclaw are often sufficient without excessive glare, requiring less frequent shading intervention. The lower part closure (state: 'down-closed') occurs 23.36% of the time, and the upper part (state: 'all-closed') is closed 7.91%, indicating a balanced approach to managing excessive illuminance near the facade. In

Tehran, the bi-sectional KSS remains open for a lesser portion of the day at 15.33%. This reflects the city's high GHI levels, necessitating more frequent shading. The lower part of the shading system ('down-closed') is closed 32.65% of the time, while the upper part (state: 'all-closed') is closed 16.62% of the time. Both periods have the longest lower and upper part closure times among all analyzed cases. In Bangkok's tropical climate, bi-sectional KSS remains open for a significant 29.21% of the time, indicating ample daylight and periods of intense sunlight requiring shading. The lower part closure is 21.08%, and the upper part closure (state: 'all-closed') is only 4.90%, reflecting the need to manage excessive illuminance, primarily in the lower part of the I due to the high angle of the sun typical in tropical regions.

Table 5. Percentage frequencies of kinetic shading system states for Wrocław, Tehran, and Bangkok. The table highlights the proportion of time each shading system state is active.

State	Wrocław (%)	Tehran (%)	Bangkok (%)
night [1]	52.83	52.02	49.71
open	23.81	15.33	29.21
down-closed	23.36	32.65	21.08
all-closed	7.91	16.62	4.90

[1]—below the threshold of detection.

Overall, the bi-sectional KSS adapts to each location's unique climatic conditions with varying degrees of openness and closure. In Wroclaw, the bi-sectional KSS often remains open due to moderate daylight, and the instantaneous levels of elevated illuminance generally govern the opening of the lower and upper parts throughout the entire year (also activated in, e.g., January). Bangkok's bi-sectional KSS remains open frequently but demonstrates a substantial need to manage excessive sunlight, particularly in winter. In Tehran, the closure of the upper part ('all-closed') is practically dependent on lower solar altitudes. In Tehran, the shading system is fully closed 16.62% of the time, significantly higher than in Wroclaw (7.91%) and Bangkok (4.90%). This suggests that Tehran experiences more intense or prolonged periods of high illuminance, necessitating complete closure of the shading system more often to manage excessive sunlight and maintain indoor comfort. This higher frequency of full closure underscores the importance of robust shading solutions in regions with high solar exposure. Figure 7 shows these variations and highlights the bi-sectional KSS's flexibility and the importance of location-specific control strategies to optimize daylight comfort and energy efficiency in diverse climatic contexts.

4.5.2. Qualitative Study: IAG

A comprehensive glare study was conducted annually for Wroclaw, Tehran, and Bangkok for a specific viewpoint coincident with sensor 'A' location. The study calculated the DGP values using the Imageless Annual Glare component in Ladybug Tools, version 1.6.0. The DGP was calculated for two configurations: (i) static fins according to the 'open' state, and (ii) dynamic fin configurations aligned with the FCS. The results demonstrated significant differences in DGP values across the configurations and locations, highlighting the critical role of KSS in managing visual comfort.

With the 'open' configuration of KSS, the highest number of hours with intolerable glare (DGP > 45%) was observed in Tehran—1652 h. Wroclaw followed with 1129 h, and Bangkok with 587 h. The different sun paths and weather patterns can explain these results. Tehran, having the clearest sky and highest irradiance values, exhibited similar hours with both imperceptible and intolerable glare. The distribution of glare hours is given in Table 6.

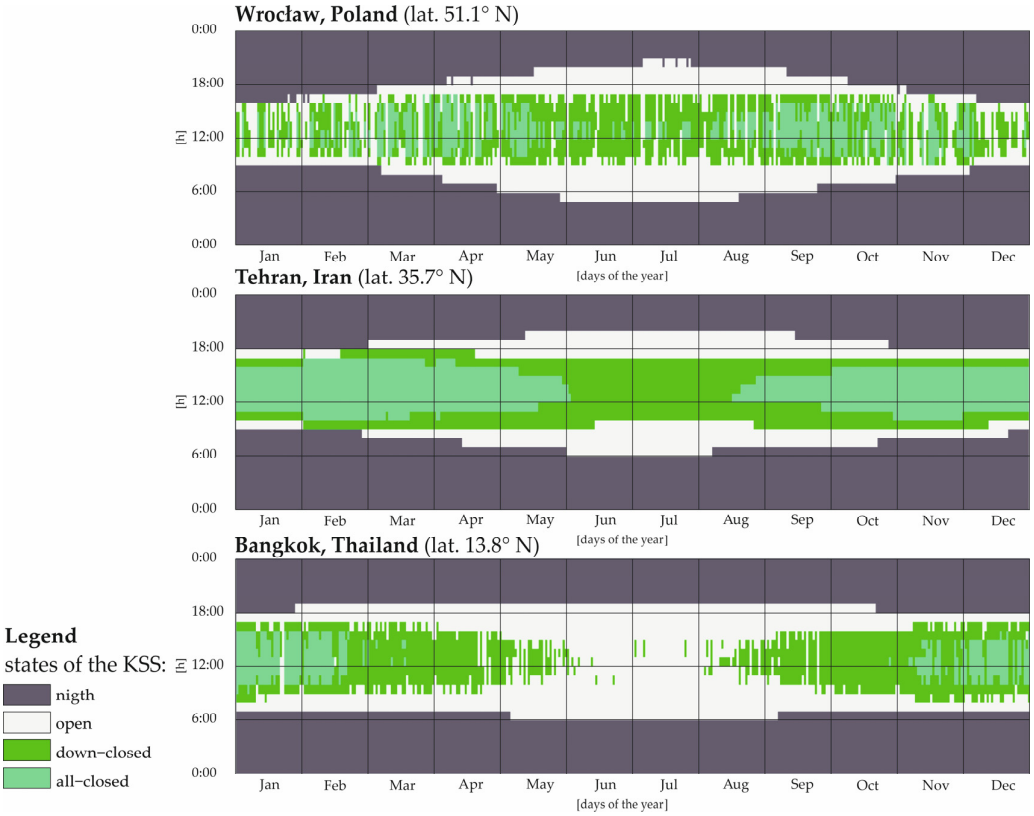


Figure 7. KSS switching schedule in Wroclaw, Tehran, and Bangkok throughout the year. This figure illustrates the time the KSS remains in each operational state—'open', 'down-closed', and 'all-closed'—across three distinct climates. Data reveal the system's adaptive responses to the specific solar and daylight conditions.

Table 6. Distribution of glare hours by DGP levels across different locations.

		Wrocław		Tehran		Bangkok	
Level of Discomfort	**DGP/**	**"Open"**	**FCS**	**Open"**	**FCS**	**"Open"**	**FCS**
Imperceptible Glare	>35%	2217	3889	1510	4109	2939	4300
Perceptible Glare	>35%<40%	413	233	509	94	465	105
Disturbing Glare	>40%<45%	373	10	532	0	414	0
Intolerable Glare	>45%	1129	0	1652	0	587	0
	Total:	4132 *	4132 *	4203 *	4203 *	4405	4405

*—negligible values of DGP are omitted (below 5%).

The 'down-closed' and 'all-closed' configurations, when switched according to the FCS, showed considerable glare reduction, with DGP values below the discomfort threshold. The application of FCS improved conditions in all locations, decreasing the number of hours with intolerable glare (DGP > 45%) to zero. This demonstrates the high effectiveness of the proposed solution across various climatic and geographical locations. See Figures 8–10.

An additional snapshot analysis was conducted on 21 March at 10 AM to capture conditions at a specific moment in the year. This analysis included one additional condition not previously studied, named 'up-closed', to assess its effectiveness in reducing glare. The 'up-closed' configuration was intentionally simulated to evaluate its potential for glare mitigation. The simulation results indicate that it has some potential for reducing glare, as evidenced by lower DGP values compared to the fully open configuration, with values of 33%, 33%, and 39% for Bangkok, Wroclaw, and Tehran, respectively. Considering that

personal override control will be available for office occupants, the 'up-closed' configuration could temporarily address momentarily high glare conditions.

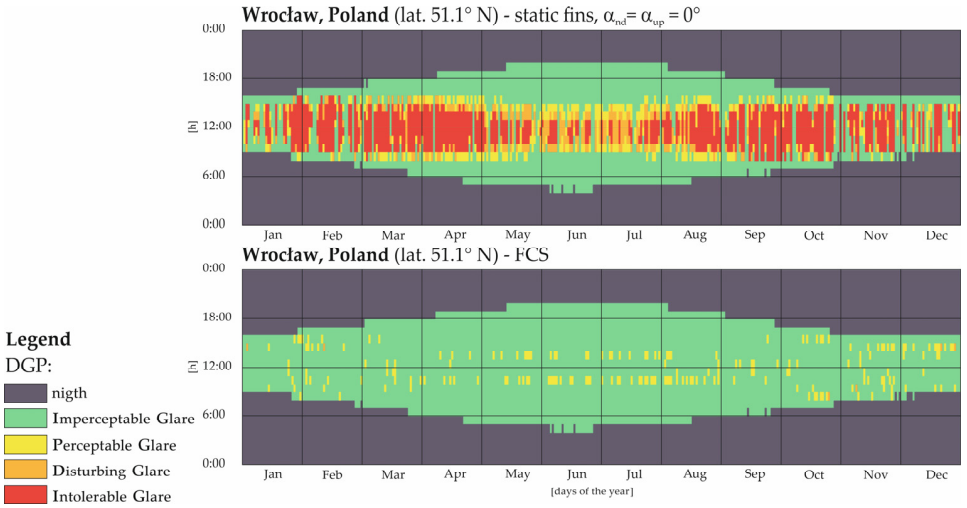


Figure 8. Annual distribution of glare hours by DGP in Wrocław.

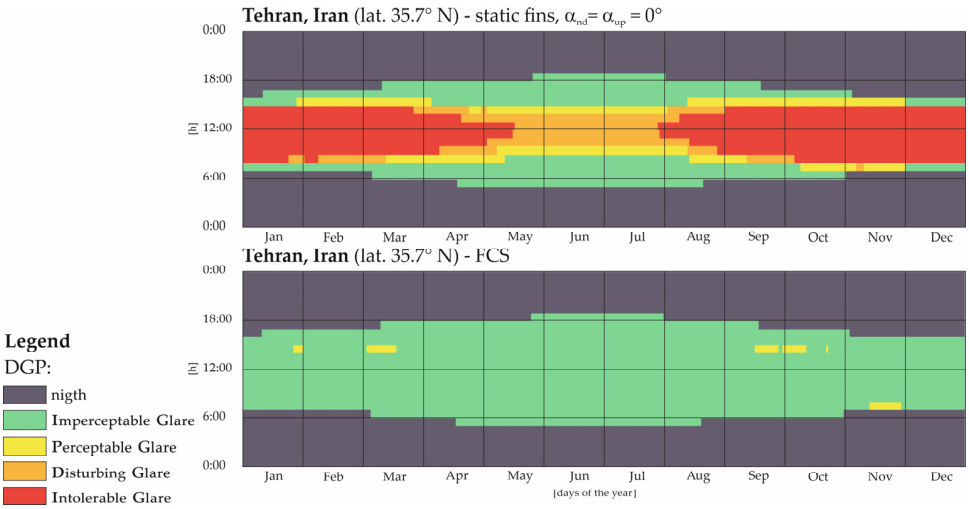


Figure 9. Annual distribution of glare hours by DGP in Tehran.

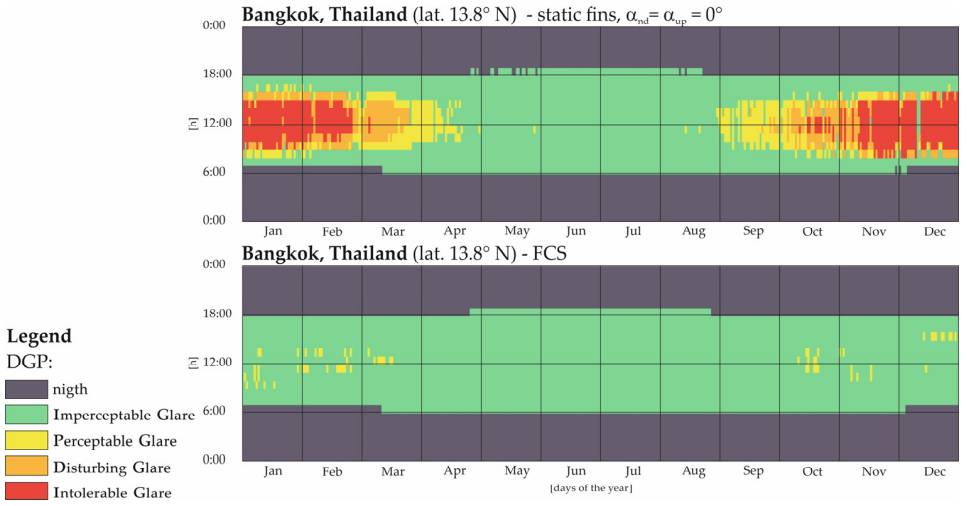


Figure 10. Annual distribution of glare hours by DGP in Bangkok.

Using bi-sectional KSS across three climate zones—Wroclaw, Tehran, and Bangkok—significantly improved indoor visual comfort.

5. Experiment

In addition to simulation studies, an experimental analysis was conducted to enhance accuracy compared to the simulation, and assess the practical feasibility of the bi-sectional KSS in real-world conditions. The experiment allowed for a significant increase in temporal resolution, from the 1-h interval used in the simulation to 2 s in the experimental setup. This finer resolution enabled the recording, visualization, and detailed observation of how the upper and lower fins adjusted based on changes in illuminance—something that would not have been possible in the simulation.

While the simulations offer predictive insights based on standardized climate data and virtual sensors, the experiment allows us to assess the KSS's effectiveness in a controlled yet realistic environment. By employing real hardware sensors and a reduced-scale mock-up, the experiment captures dynamic responses to natural light variations that are often difficult to replicate in simulations. These empirical data reinforce the simulation results' accuracy and highlight the KSS's robustness in maintaining optimal daylight levels and reducing glare under real-world conditions. Additionally, the experiment offers insights into the operational challenges and potential refinements needed for practical implementation, which are not always evident in simulation models alone.

The experimental setup involved installing a mock-up of bi-sectional KSS in an office environment and measuring its performance under varying lighting conditions. It must be explicitly stated that the experimental study was conducted in Wrocław, Poland only. Wrocław has a temperate climate, representing a wide range of mid-latitude locations. Additionally, Wrocław was selected to ensure consistency with the author's previous research in the exact location [10], thereby building a more comprehensive understanding of KSS over time.

5.1. Experiment Design and Method

A physical modelling experiment evaluated daylight performance in real-world conditions and compared the results with simulation data. This method is commonly used in architecture and engineering to simulate physical phenomena under controlled conditions. Reduced-scale mock-ups have proven successful in evaluating daylight performance, as demonstrated by Mandalaki and Tsoutsos (pp. 83–86) [48], with similar approaches presented by Bahdad et al. [49] and Zazzini et al. [50].

The experiment used a custom-made, reduced-scale mock-up (1:20) of the Test Room, consisting of two chambers: Chamber '1', where the bi-sectional KSS was installed, and Chamber '2', a fully glazed control room without any shading system. The mock-up was equipped with two daylight illuminance sensors, A_1 and A_2 (BH-1750 manufact. by Rohm Semiconductors, Kyoto, Japan [51]), connected to a Raspberry Pi 3, which controlled the shading fins in real-time based on illuminance data. Data were collected at 2-s intervals to enable detailed tracking of daylight conditions. Additionally, two Testo THL 160 data loggers (manufact. Testo SE & Co. KGaA, Titisee-Neustadt, Germany.) were installed to monitor illuminance in the middle—sensor B—and at the back—sensor C—of Chamber '1'.

Weather conditions were monitored using data from the nearest meteorological station, with irradiance measured by a CM 11 pyranometer (manufact. Kipp and Zonen, Delft, Netherlands) at the Meteorological Observatory of the Department of Climatology and Atmosphere Protection, Wrocław University (51°06′19.0″ N, 17°05′00″ E, elevation: 116.3 m) [52].

The mock-up was located in Wrocław, Poland (51.1079° N latitude, 17.0385° E longitude). According to the Köppen climate classification, Wrocław's climate is primarily oceanic (Cfb), bordering on a humid continental climate (Dfb), using the 0 °C isotherm. Essential climate data for Wrocław were derived from the WMO Guidelines on the Calculation of Climate Normals, WMO-1203 [53].

The KSS system dynamically adjusted its fins based on real-time illuminance readings, with a target illuminance level set at 3000 lx and a hysteresis range of 300 lx to prevent constant adjustments. Specifically, the system maintained illuminance levels between 2700 and 3300 lx. The Raspberry Pi-controlled motors adjusted the fins between 0° and 60° to ensure optimal lighting. Unlike the simulation studies mentioned earlier, the automated control software allowed for smooth transitions of the fins within this range, as postulated by Carlucci et al. [35].

An advanced algorithm embedded in a Python script was developed to optimize the E_{h1} values using a prototype of the KSS, with key thresholds set for the target value and hysteresis. This algorithm was based on an earlier simulation model (Figure 3) and was inspired by the work of Al-Obaidi et al. [54].

The mock-up was installed indoors, behind a large glazed window, to simulate realistic solar radiation conditions while protecting the setup from external weather influences. Data collection primarily occurred during peak sunlight hours, from 1 PM to 6 PM, capturing the system's response to direct sunlight.

For brevity, detailed descriptions of materials and equipment, including specifics on sensors and motors, are provided in the Supplementary Materials (see Supplementary_Data_S2.pdf). The Supplementary Materials also include:

- Complete data collection methods, variables, and the data analysis plan;
- Tables with detailed climate data and measuring equipment characteristic;
- Results from preliminary and pilot studies of the mock-up's initial testing;
- Full details of the control algorithm and technical aspects of the Raspberry Pi control system;
- A discussion of experiment limitations and mitigation procedures;
- Photographs of the experimental setup.

5.2. Experiment Results

This section presents the results of the bi-sectional KSS experiment across three time scales to verify its effectiveness in real-world conditions. Three days were chosen to represent different weather patterns: a clear day, a day with scattered clouds, and an overcast day. Irradiance data were recorded at 60-min intervals, while illuminance data from sensors in Chambers '1' and '2' were recorded at 1-min intervals during peak solar radiation (1 PM to 6 PM). For a more detailed analysis of KSS efficiency, illuminance measurements were tracked at 2-s intervals between 1 PM and 4 PM, allowing for the observation of the fins' dynamic behavior.

5.2.1. Sixty-min Intervals: Irradiance Analysis

Three days were selected based on irradiance data. The selection was based on the values of total irradiance (I_t) and diffuse irradiance (I_d), and clearness index K_t calculated according to Duffie and Beckman [55]:

- Day 1 (29 June 2024)—scattered clouds, K_t = 0.939.
- Day 2 (6 July 2024)—clear day, K_t = 1.0.
- Day 3 (7 July 2024)—overcast, K_t = 0.432.

Irradiance analysis revealed that, on clear days, the mean total irradiance (I_t) was 309 W/m^2, with a maximum of 881 W/m^2. On overcast days, the mean I_t dropped to 134 W/m^2, while diffuse irradiance (I_d) increased due to cloud scattering. The highest I_d recorded was 378 W/m^2 on overcast days, compared to 248 W/m^2 on clear days. These differences in irradiance underscore the diverse performance of the bi-sectional KSS under various weather conditions (see Figure 11). Box plots revealed distinct differences in irradiance patterns between selected analysis days, supporting the analysis of the bi-sectional KSS performance in diverse weather conditions (see Appendix B).

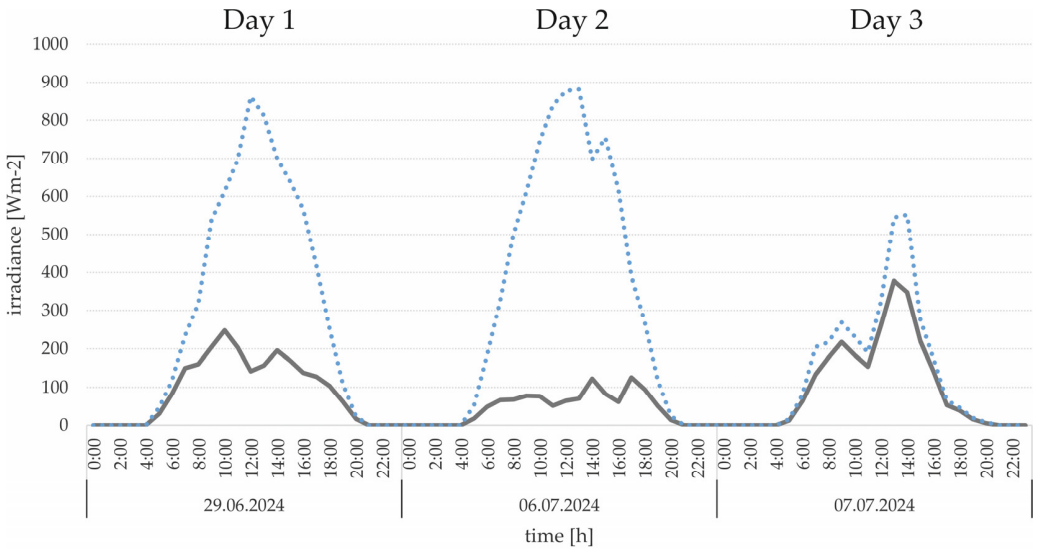


Figure 11. Irradiance measurements for the analysis days: Day 1, Day 2, and Day 3. The dotted blue line indicates total irradiance (I_t), and the grey line indicates diffuse irradiance (I_d). The measurements were recorded at the closest Meteorological Observatory of the Department of Climatology and Atmosphere Protection, Wrocław University (51°06′19.0″ N, 17°05′00″ E, elevation: 116.3 m) [52].

5.2.2. One-min Intervals: Illuminance Measurements from Sensors 'A_1' and 'A_2'

Illuminance levels in Chambers '1' and '2' were compared, respectively, denoted E_{h1} and E_{h2}. On a clear day (6 July), Chamber '2' (without protection) reached up to 67,000 lx, while Chamber '1' (with KSS) had significantly lower levels, indicating effective glare reduction. The KSS maintained the room's set illuminance values, with E_{h1} values peaking at 4674 lx on Day 1, 3973 lx on Day 2, and 3588 lx on Day 3. Despite occasional peaks exceeding the 3000 lx threshold, the system effectively controlled daylighting, as shown by standard deviations of 537 lx, 377 lx, and 214 lx for each respective day (see Figure 12).

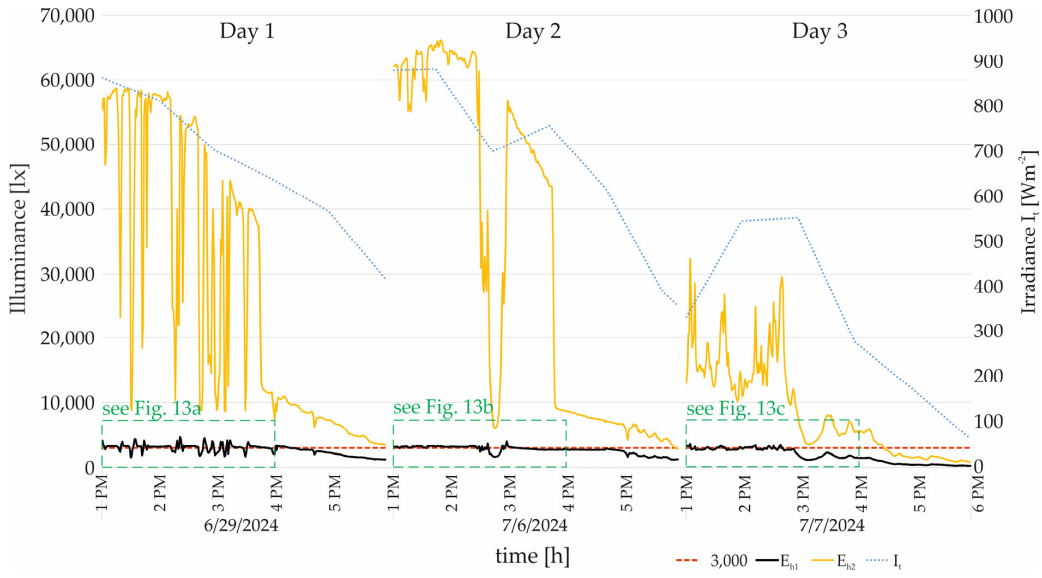


Figure 12. E_{h1} and E_{h2} measurements from 1 PM to 6 PM for all analysis days. The yellow line shows E_{h2} (Chamber '2', no protection), and the black line shows E_{h1} (Chamber '1', behind KSS). The blue dotted line represents total irradiance (I_t) from the weather station, and the red dashed line marks the 3000 lx trigger threshold. The green dashed outline indicates the area enlarged in the next section in Figure 13a–c.

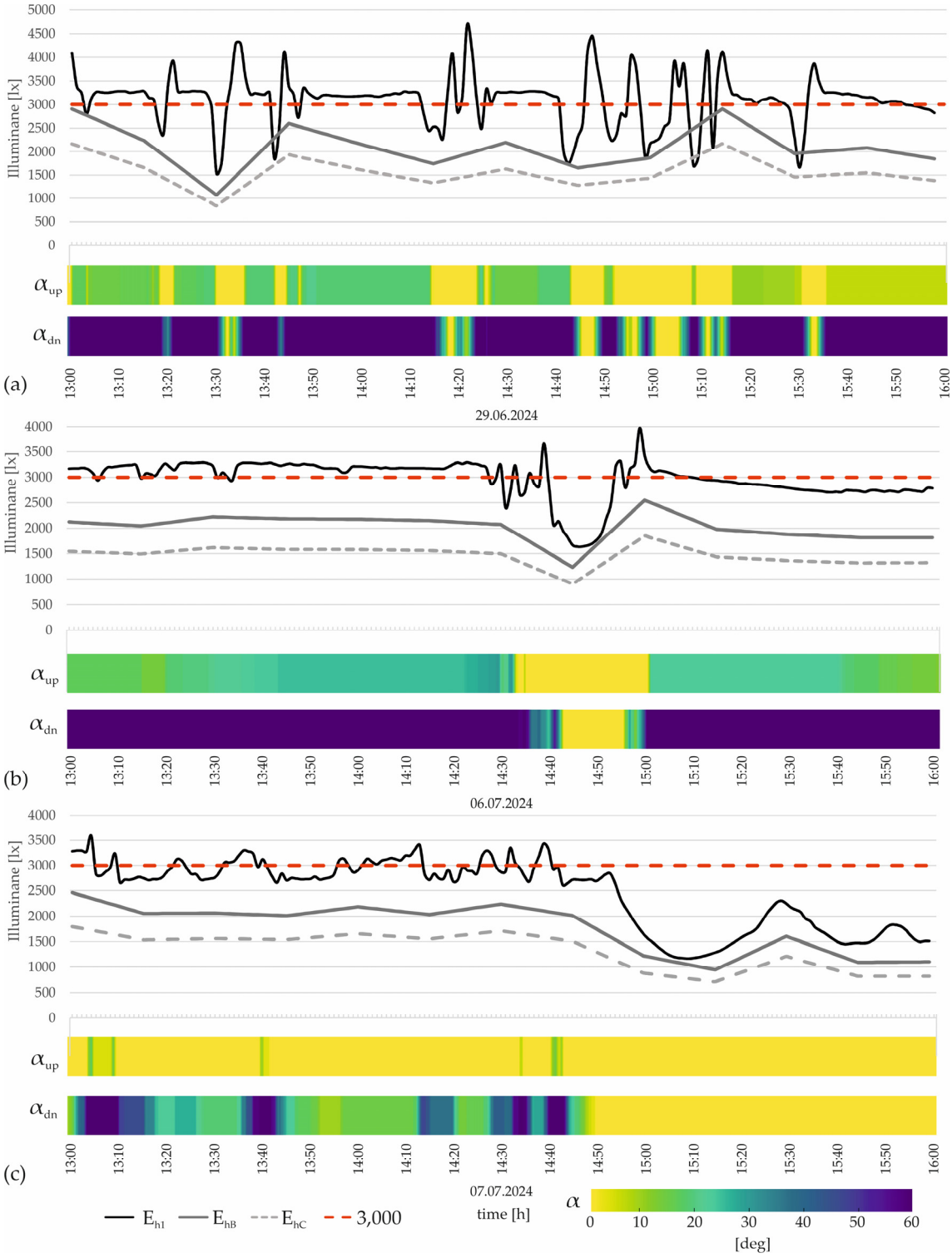


Figure 13. Detailed analysis of illuminance measurements in Chamber '1' (behind the KSS) from 1 PM to 4 PM for Days 1, 2, and 3. The black line shows E_{h1}, while the grey lines (continuous and dashed) represent E_{hB} and E_{hC}, measured by sensors 'B' and 'C' in the middle and back of the room, respectively. The red dashed line represents the 3000 lx threshold. Heatmaps illustrate the dynamic behavior of the bi-sectional KSS, with yellow indicating fully open fins ($\alpha = 0°$) and blue indicating fully closed fins ($\alpha = 60°$).

5.2.3. Two-s Intervals: Illuminance Measurements from Sensors 'A_1', 'B', and 'C'

At the finest scale, the illuminance data from sensors in the middle and back of Chamber '1' (sensors 'B' and 'C') were analyzed. E_{h1} exhibited more variability due to more frequent sampling compared to E_{hB} and E_{hC}. The bi-sectional KSS's dynamic adjustments are illustrated in heatmaps, showing how the fins reacted to varying illuminance levels.

- Day 1: Scattered clouds led to variable illuminance, with E_{h1} ranging from 4674 to 1541 lx. The lower fins adjusted between 0° and 60°, while the upper fins adjusted from 0° to 20°, ensuring sufficient daylight penetration and maintaining comfort levels, as the illuminance at the back of the room never dropped below 300 lx.
- Day 2: Illuminance remained stable, with E_{h1} between 3973 and 1638 lx. The lower fins stayed mostly closed (60°) except for brief adjustments, and the upper fins followed a similar pattern, ensuring light levels were within the desired range.
- Day 3: Overcast conditions resulted in lower E_{h2} values, yet the KSS maintained proper E_{h1} levels between 3588 and 1171 lx. The lower fins dynamically adjusted until 2:45 PM, remaining open as the irradiance dropped. This adjustment reduced the illuminance by a factor of 5.57 compared to the external readings (see Figure 13).

By illustrating the range of fin movements (from fully open to fully closed) across different lighting scenarios, the heatmaps offer unique insights into the system's real-time responsiveness, which cannot be fully captured by numerical data alone. This visual information is crucial for understanding the KSS's efficiency and adaptability in diverse weather conditions, making it a valuable contribution to the overall analysis.

A comprehensive set of experimental results is presented in Supplementary Materials (see Supplementary_Data_S2.pdf).

6. Discussion

The simulation and measurement data presentation opens a path for a discussion regarding the effectiveness of the presented bi-sectional KSS. It is important to note that the simulations were conducted for three different climate zones (Wrocław, Tehran, and Bangkok), while the experimental measurements were carried out in Wrocław due to practical considerations related to the university's location.

6.1. Effectiveness of KSS

The effectiveness of the bi-sectional KSS must be analyzed across various temporal scales, depending on the applied methodology.

6.1.1. Simulation Study

Yearly simulations demonstrate that the bi-sectional KSS consistently maintains illuminance levels between 300 and 3000 lx ($UDI_{300–3000}$), with an average improvement:

- Over rooms without any shading: 61.40% for Wrocław, 148.60% for Tehran, and 88.53% for Bangkok (the elevated value for Bangkok is due to the very low values of $UDI_{300–3000}$ for the facade without any shading). In all climate scenarios, the bi-sectional KSS outperformed the room without any shading systems by an average of 99.39% in daylight distribution, as derived by comparing statistical metrics.
- Over rooms with static shading in the 'open' state: 31.96% for Wrocław, 54.69% for Tehran, and 37.05% for Bangkok (average 41.23%).

The bi-sectional KSS effectively manages illuminance levels within the range of 300 to 3000 lx ($UDI_{300–3000}$), regardless of the climate. These results indicate that the bi-sectional KSS significantly enhances daylight distribution in the room, with all quantitative metrics showing improved values. The simulated performance in terms of the daylight metric should be put into context. The results of the presented study for cities with lower latitudes are at approximately the same level as the average KSS performance improvement of 46.8% (in daylight) or 43.3% (in energy) derived from the review study of sixty-six case studies of KSS from 2022 to 2024, recently published by the author [17]. Additionally, the performance

improvement was higher than the 26.2% estimated in 2014 by Han [56]. In 2019, Lee developed an optimal positioning algorithm for kinetic shading devices to minimize total energy demands and arrived at energy savings of 28.7% in Abu Dhabi, 28.2% in Hanoi, and 23.8% in Seoul [57].

Although the qualitative results remain heavily dependent on solar altitude, a specific configuration of the bi-sectional KSS, 'up-closed', proved effective in mitigating glare at selected times of the day, lowering the Daylight Glare Probability (DGP) by 27.65%.

The study of KSS switching schedules allowed for the tracking of the characteristic features of the bi-sectional KSS in different climates. In a temperate climate (Wrocław), the closure of the bi-sectional KSS—especially in the 'all-closed' state—heavily depends on instantaneous 'blinks' of direct sunlight, occurring in both June and January. The analysis revealed that in Wrocław, the 'all-closed' state was triggered 20 times in June and 25 times in January due to instantaneous sunlight blinks. In hot and arid climates (Tehran), the bi-sectional KSS switching schedule is primarily governed by high solar altitude due to predominantly clear sky conditions. In hot and humid climates (Bangkok), overcast conditions persist throughout the summer months, resulting in the full closure of the bi-sectional KSS only in winter, when solar altitudes are relatively low. In all analyzed cases, the same FCS was used to achieve the reported improvements, which contradicts the conclusion of the study by Norouziasas et al., who claimed that "fixed schedules may not adapt well to dynamic conditions" [32].

6.1.2. Experimental Study

Experiments assessed bi-sectional KSS performance over different time scales. The KSS effectively maintained illuminance levels below 3000 lx in Chamber '1' for 68% of the time, despite higher levels in Chamber '2'. Peaks up to 4500 lx were recorded and discussed in detail in Supplementary Materials (see Supplementary_Data_S2.pdf). The analysis, limited by sensor numbers and duration, sacrificed simulation length for higher temporal resolution.

Hourly data (1 PM to 6 PM) showed the KSS adapted well to changing conditions, maintaining visual comfort and reducing glare. In a detailed 3-h analysis (1 PM to 4 PM), sensors 'B' and 'C' at the back of the room recorded illuminance consistently above 300 lx, proving the effectiveness of the dual fin design.

The algorithm dynamically adjusted the fins on a finer scale to maintain consistent lighting. Heatmaps show lower fins rotated between 0° and 60°, adjusting 44 times, while upper fins moved within 0°–25°, adjusting 76 times. Day 1 showed the highest variability due to cloud cover, with a standard deviation of 537 lx, highlighting the system's lag in response to rapid irradiance changes.

While not the primary focus, a comparison between E_{h1} (Chamber '1' with KSS) and E_{h2} (Chamber '2' without protection) showed the KSS reduced illuminance by a factor of 7.94, demonstrating its effectiveness in reducing daylight intensity. However, this factor is limited by sensor positioning and does not fully reflect room conditions. The bi-sectional KSS would significantly improve occupant comfort by reducing excessive brightness and maintaining adequate lighting for office tasks. A full discussion of the results of the experimental study is presented in Supplementary Materials (see Supplementary_Data_S2.pdf).

7. Conclusions

The presented paper discussed the bespoke bi-sectional KSS system performance using simulation and experimental verification.

7.1. Main Points

- The initial part of the paper presented a "State of the Art" study conducted to show critical trends in the research dedicated to KSS. This information provided the background for considering the original, bespoke, bi-sectional KSS, providing insight into existing work, field gaps, and improvement opportunities.

- Both simulation and experimental studies proved that bi-sectional KSS significantly improves daylight distribution and uniformity across diverse climate zones (Wroclaw, Tehran, and Bangkok—31.96%, 54.69%, 37.05%, respectively vs. the scenario with static fins). Simulations show increased $UDI_{300–3000}$ values, enhancing visual comfort by maintaining optimal illuminance levels.
- The bi-sectional KSS reduces the maximum illuminance and glare potential within office spaces. Simulations indicate that the system maintains illuminance within the comfort range for more time than unshaded or statically shaded systems, improving visual comfort metrics significantly.
- The bi-sectional KSS was experimentally verified to dynamically adjust to varying solar conditions, providing better protection and comfort during different times of the day and under various weather conditions. This dynamic adaptation helps mitigate the impact of excessive sunlight and glare, particularly in high solar exposure regions like Tehran.
- By maintaining daylight illuminance levels between 300 and 3000 lx, and reducing reliance on artificial lighting and cooling, the bi-sectional KSS can potentially achieve energy savings. These limits are based on established standards, such as those from LEED v.4, which aim to minimize artificial lighting use while preventing glare and excessive solar heat gain. Although the research in the paper was focused on visual comfort metrics and did not calculate solar heat gain, it might be speculated that bi-sectional KSS minimizes the need for air conditioning. This promotes sustainable building practices and reduces the carbon footprint of buildings.
- The study advocates for the broader application and further development of bi-sectional KSS in various architectural contexts. The system's ability to enhance visual comfort and energy efficiency under different climatic conditions underscores its potential as a viable solution for sustainable building design.

Additionally, the manuscript provides a rare illustration of the operational dynamics of the KSS, showing switching schedules for simulations and detailed heatmaps for experiments. These visualizations offer valuable insights into the practical implementation and effectiveness of the KSS.

7.2. Key Findings

- Effectiveness Across Climates: The study demonstrates that the bi-sectional kinetic shading system (KSS) significantly enhances daylight comfort across diverse climates—Wrocław, Tehran, and Bangkok—by optimizing daylight levels and reducing solar heat gain.
- Improved Visual Comfort: The KSS improves visual comfort by maintaining illuminance levels below discomfort thresholds, particularly in reducing glare, as shown by the lower Daylight Glare Probability (DGP) in various configurations.
- Experimental Validation: The experimental results support the simulation findings, demonstrating the robustness of the KSS in real-world conditions, especially during high-illuminance periods.

7.3. Unique Contributions

- Innovative Bi-Sectional Design: The introduction of the bi-sectional KSS, allowing independent control of upper and lower fins, is a novel approach in kinetic shading systems, offering precise daylight management tailored to varying climatic conditions.
- Dual Methodology: The combination of simulation and experimental approaches provides a comprehensive evaluation of the KSS's performance, enhancing the reliability and applicability of the findings.
- Custom Metrics and Control Algorithms: The study introduces custom metrics for evaluating daylight performance and a novel control algorithm that dynamically adjusts the KSS based on real-time illuminance data, contributing to the field of adaptive facade technology.

7.4. Limitations of Study

This study has some explicit limitations that should be acknowledged. First, the simulation was limited to three locations; other locations with different climates and weather patterns might yield different results. Second, the inherent properties of the Radiance engine limit the temporal resolution of the simulation study to one hour, which might not capture all weather phenomena accurately. Third, the *.epw files used for the simulation may need to be updated to reflect current climate changes, such as sunnier periods. Fourth, the experiment was conducted over a limited timeframe, from 28 June to 15 July 2024, due to factors beyond the author's control, providing reliable measurement results primarily after 1 PM, reflecting peak irradiance levels. Fifth, the lower fins in the bi-sectional KSS may have compromised the horizontal view angle (14° to 28°) required by the European Standard EN17037 for occupants in a sitting position. Sixth, the horizontal design of the KSS might be threatened by natural forces such as wind and snow in temperate climates, potentially affecting its integrity.

7.5. Future Research

The proposed bi-sectional KSS could be further investigated within a different experimental timeframe, reflecting daylight conditions on days with shorter durations of sunlight and overcast conditions. The experiment's parameters might be further refined by changing the recommended illuminance range, for example, 300–2000 lx, or adjusting the hysteresis to 600 lx. Combined solutions with horizontal fins at different heights are another option to explore. This paper does not compare the cost-effectiveness of the bi-sectional KSS variants, which is a significant omission given the potential financial implications. Future research could examine the bi-sectional KSS's cost and finance aspects to provide a more comprehensive analysis. Enhancing the adaptability and responsiveness of the bi-sectional KSS should also be studied by tuning the parameters of the experimental setup. A possible improvement is adopting a different geometry for the shading system that is resistant to snow accumulation.

7.6. Key Takeaway

The bi-sectional KSS is highly effective in enhancing visual comfort across diverse climatic conditions, making it a climate-responsive solution for sustainable and adaptive building designs.

Supplementary Materials: The following supporting information can be downloaded at: https://www.mdpi.com/article/10.3390/su16188156/s1: Supplementary_Data_S1.xlsx, Supplementary_Data_S2.pdf.

Funding: The electronic components used to build the control system for KSS, which includes Raspberry Pi 3, BH-1750 sensors, and stepper motors as part of the experimental study, were purchased with funds from Wrocław University of Science and Technology with current assets.

Institutional Review Board Statement: Not applicable.

Informed Consent Statement: Not applicable.

Data Availability Statement: The raw data supporting the conclusions of this article will be made available by the author on request.

Acknowledgments: The author wishes to thank Magdalena Baborska-Narożny, Wroclaw University of Science and Technology, for lending the Testo THL-160 data loggers used for the measurements in the paper, and Maciej Kryza for making the weather data available from the weather station of the Meteorological Observatory of the Department of Climatology and Atmosphere Protection, Wrocław University (51°06′19.0″ N, 17°05′20.0″ E, elevation: 116.3 m). I also want to thank Tomasz Malek, whose technical expertise and dedicated assistance were invaluable in developing the Python script essential for running the prototype presented in this paper. I am deeply grateful for his support and generosity in sharing his profound knowledge and time. Also, I would like to express my gratitude to Stanisław Brzezicki for his invaluable assistance in developing the KSS flowchart used in this study.

Conflicts of Interest: The author declares no conflicts of interest.

Nomenclature

Metric	Unit	Description
ASE	[h]	Annual Solar Exposure
CBDM	n.a.	Climate-Based Daylight Modelling
DGP	[%]	daylight glare probability
DSIM	n.a.	*Discrete state illumination method*
E_h	[lx]	Horizontal illuminance
E_{h1}	[lx]	Horizontal illuminance at sensor A_1
E_{h2}	[lx]	Horizontal illuminance at sensor A_2
E_{hB}	[lx]	Horizontal illuminance at sensor B
E_{hC}	[lx]	Horizontal illuminance at sensor C
E_{max}	[lx]	Maximum illuminance at the sensor 'A_1'.
FSC	n.a.	Façade Closure Scheme
GHI	Wm^{-2}	Global Horizontal Irradiance
I_d	Wm^{-2}	Diffuse Irradiance
I_t	Wm^{-2}	Total Irradiance
K_t	n.a.	Clearness Index
KSS	n.a.	Kinetic Shading System
Mdn_{Eh}	n.a.	Median illuminance in the year at the sensor 'A'.
$t_{<300}$	[h]	Hours per year with illuminance below 300 lx at sensor 'A'.
$t_{>3000}$	[h]	Hours per year with illuminance over 3000 lx at sensor 'A'.
UDI	[%]	Useful Daylight Illuminance
U_{UDI}	n.a.	UDI uniformity for final $UDI_{300–3000}$ distribution
σ_{UDI}	n.a.	Standard deviation σ for final $UDI_{300–3000}$ distribution
$\widetilde{m}_{UDI}$	n.a.	Median for the final $UDI_{300–3000}$ distribution
UDI_{max}	[%]	The maximal UDI for the final $UDI_{300–3000}$ distribution
$\overline{UDI}$	[%]	Average UDI for final $UDI_{300–3000}$ distribution
DA	[%]	Daylight Autonomy
U_{DA}	n.a.	DA uniformity for the final DA_{500} distribution
σ_{DA}	n.a.	Standard deviation σ for final DA_{500} distribution
$\widetilde{m}_{DA}$	n.a.	Median for the final DA_{500} distribution
DA_{max}	[%]	The maximal DA for the final DA_{500} distribution
$\overline{DA}$	[%]	Average DA for final DA_{500} distribution
'S'	n.a.	KSS state
IQR	n.a.	Interquartile Range
R^2	n.a.	R-squared, Coefficient of determination
$\bar{e}$	[lx]	Mean Error
CV(RMSE)	[%]	Coefficient of Variation of the Root Mean Square Error

Appendix A

The daylight simulation method used in the paper is called Climate-Based Daylight Modeling. This method simulates and analyses the impact of daylight within buildings, considering specific climatic conditions. The calibration method is grounded in logical reasoning, beginning with the assumption that accurate simulation validation requires alignment with real-world conditions. The software's historical weather data often diverge from current conditions, potentially leading to simulation inaccuracies. Therefore, the author modifies the simulation input files (*.epw) to reflect real-time data collected during experiments to achieve meaningful comparisons. This approach is supported by studies demonstrating improved simulation accuracy when using actual/contemporary data. Bupi et al. used a method which "updates its database with recent data, allowing for accurate simulations of photovoltaic power outputs" [58]. Loutzenhiser et al. used "weather data measured at the facility (...) in 10 min intervals as boundary conditions" [59]. Mazzeo et al. presented the most similar approach, comparing and validating simulations in EnergyPlus, IDA ICE, and Trnsys vs. experimental data by constructing custom-made *.epw files.

The authors state that weather data "were employed to build the experimental *.epw file required by EnergyPlus" [60]. Although some might argue that historical data suffice, this method accounts for unexpected anomalies, ensuring a more reliable outcome. Thus, the logical foundation of the method effectively enhances the validity of simulation results.

After the simulated illuminance values are produced, the calibration method is based on the presentation of calibration and error charts, see Figure A1, followed by the calculation of the accuracy indexes: R^2, mean error $\bar{e}$, and *CV(RMSE)*. The coefficient of variation of the root mean square error *CV(RMSE)* used as a benchmark in the presented study is supported by two main pillars: (i) literature support and (ii) previous applications. The method is grounded in established practices found in recent papers on the application of KSS, such as those by Norouzias et al. [32], Wang et al. [61], and Takhmasib et al. [62]. This method is widely recognized and utilized in similar studies. It has been successfully proved by Cacabelos et al. [63], Ascione et al. [64], and Royapoor and Roskilly [65], demonstrating its feasibility and reliability in comparable contexts. These studies provide evidence of the method's effectiveness and support its use in the present work.

Due to the relatively short measurement period, the calibration of the model was verified based on data collected on ten days, from 28 June to 3 July and 6 July to 9 July. During these times, the experimental setup worked with a threshold of 3000 lx and a hysteresis of 300 lx. The exclusion of 4 and 5 July was necessary due to a power outage beyond the author's control. The calibration period spans ten days, encompassing a variety of weather patterns. As explained above, a bespoke weather file was created using real measured weather data from the calibration period.

Due to different temporal scales, the collected 2-s measurements denoted as E_{h1} were averaged to show the mean value for each hour from 1 PM to 6 PM and further processed as the 'observed values'. The 'predicted values', denoted as E_h, were simulated for virtual sensor 'A' according to the procedure described in Section 4.1, using real weather data (I_t and I_d) measured in the period of ten days: 28 June to 3 July and 6 July to 9 July local weather station by updating the *.epw file [52].

The predicted E_h and observed E_{h1} values were compared, and the calibration chart is presented in Figure A1a. The blue points generally follow the red dashed line, indicating that the simulated values closely match the measured values. This suggests that the simulation model effectively captures the overall trend in the data. The R-squared (R^2) value, a statistical measure indicating how well the predicted values approximate the actual measured values, was calculated to be 0.914. An R^2 value of 0.914 indicates that 91.4% of the variance in the observed values can be explained by the predicted values, demonstrating a strong correlation between the two datasets. This suggests that the simulation model performs well in capturing the underlying pattern of the measured values.

Additionally, the calibration error values are presented in Figure A1b. The mean error of approximately 50.39 indicates that, on average, the simulated values differ from the measured values by this amount. The model tends to overestimate (negative errors) or underestimate (positive errors) the measured values, primarily at the beginning of the observation period, around 1 PM. This discrepancy may be attributed to sudden, intense sunlight bursts detected by the sensor but not accurately reflected in the simulation, which operates on an hourly temporal resolution.

To further verify the model, the *CV(RMSE)* was calculated and found to be 18.74%, according to the following formulas:

$$RMSE = \sqrt{\frac{1}{n}\sum_{i=1}^{n}(obs_i - pre_i)^2} \quad \text{(A1)}$$

$$CV\ (RMSE) = \frac{RMSE}{\frac{1}{n}\sum_{i=1}^{n} obs_i} \times 100 \quad \text{(A2)}$$

where obs_i indicates observed values and pre_i predicted. This value supports the model's accuracy, as it falls well within the acceptable standard of less than 30%. ASHRAE Guide-

line 14–2014 states that "typically, models are declared to be calibrated if they produce *CV(RMSE)*s within ±30% when using hourly data" [66]. Although these requirements apply to computational models for energy, the author applied them to daylight in the face of the absence of specific regulations regarding daylight models.

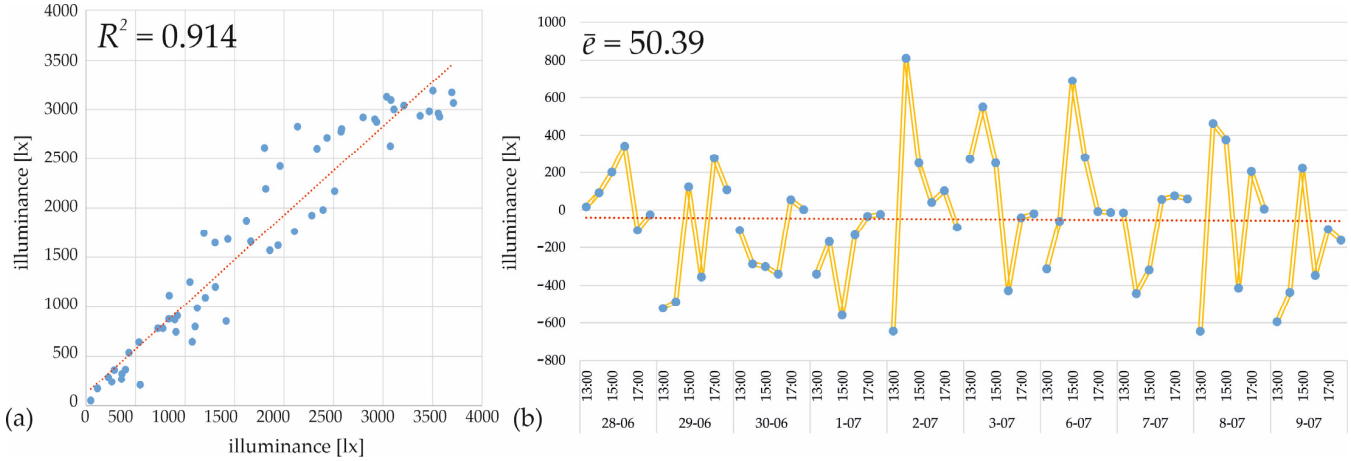


Figure A1. (**a**) a calibration chart compares predicted and observed values, demonstrating the model's accuracy in capturing the overall trend of the measured data; (**b**) an error values chart displays the differences between predicted and measured values. The chart highlights the model's performance, with particular emphasis on the variability of errors, including overestimations and underestimations, primarily observed at the beginning of the observation period at 1 PM. Red dotted line represents the trend line.

The calibration chart demonstrates a strong correlation between measured and simulated values, with an R^2 value of 0.914, indicating that the simulation captures 91.4% of the variance in the measured data, reflecting a good model fit. The *CV(RMSE)* of 18.74% further indicates that the prediction errors are relatively small compared to the mean of the measured values. Overall, the model demonstrates a high level of predictive accuracy, effectively capturing the key trends in the data. While there is some potential for refinement to address minor discrepancies, these do not detract from the model's overall strong performance.

Appendix B

Box plots reveal distinct differences in irradiance patterns between selected analysis days, supporting the analysis of the bi-sectional KSS performance in diverse weather conditions on Day 1, Day 2 and Day 3. See Figure A2.

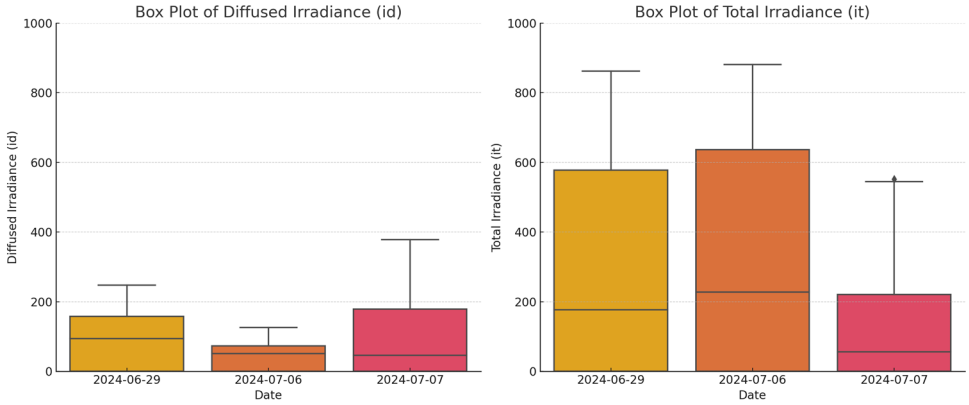


Figure A2. Box plots of I_d and I_t values illustrate diverse weather patterns on analysis days.

References

1. Thewes, A.; Maas, S.; Scholzen, F.; Waldmann, D.; Zürbes, A. Field study on the energy consumption of school buildings in Luxembourg. *Energy Build.* **2014**, *68*, 460–470. [CrossRef]
2. Sustainable Development Goals, United Nations Department of Global Communications. May 2020. Available online: https://www.un.org/sustainabledevelopment/wp-content/uploads/2019/01/SDG_Guidelines_AUG_2019_Final.pdf (accessed on 1 June 2024).
3. IPCC. Summary for Policymakers. In *Climate Change 2023: Synthesis Report. Contribution of Working Groups I, II and III to the Sixth Assessment Report of the Intergovernmental Panel on Climate Change*; Core Writing Team, Lee, H., Romero, J., Eds.; IPCC: Geneva, Switzerland, 2023; pp. 1–34. [CrossRef]
4. Daylight. U.S. Green Building Council. Available online: https://www.usgbc.org/credits/healthcare/v4-draft/eqc-0 (accessed on 1 June 2024).
5. Negroponte, N. *Soft Architecture Machines*; MIT Press: Cambridge, MA, USA, 1976.
6. Grobman, Y.; Capeluto, I.; Austern, G. External Shading in Buildings: Comparative Analysis of Daylighting Performance in Static and Kinetic Operation Scenarios. *Archit. Sci. Rev.* **2017**, *60*, 126–136. [CrossRef]
7. Ahmed, M.; Abdel-Rahman, A.; Bady, M.; Mahrous, E.; Suzuki, M. Optimum Energy Consumption by Using Kinetic Shading System for Residential Buildings in Hot Arid Areas. *Int. J. Smart Grid Clean Energy* **2016**, *5*, 2. [CrossRef]
8. Minor, J.E. Windborne Debris and the Building Envelope. *J. Wind Eng. Ind. Aerodyn.* **1994**, *53*, 207–227. [CrossRef]
9. Yi, H.-J.; Kim, D.; Kim, Y.; Kim, D.; Koh, J.-S.; Kim, M.-J. 3D-Printed Attachable Kinetic Shading Device with Alternate Actuation: Use of Shape-Memory Alloy (SMA) for Climate-Adaptive Responsive Architecture. *Autom. Constr.* **2020**, *114*, 103151. [CrossRef]
10. Brzezicki, M. Daylight Comfort Performance of a Vertical Fin Shading System: Annual Simulation and Experimental Testing of a Prototype. *Buildings* **2024**, *14*, 571. [CrossRef]
11. Alzoubi, H.H.; Al-Zoubi, A.H. Assessment of building facade performance in terms of daylighting and the associated energy consumption in architectural spaces: Vertical and horizontal shading devices for southern exposure facades. *Energy Convers. Manag.* **2010**, *51*, 1592–1599. [CrossRef]
12. Cecchi, M.; Naticchia, B.; Carbonari, A. Development of a first prototype of a liquid-shaded dynamic glazed facade for buildings. *Creat. Constr. Conf.* **2014**, *85*, 94–103. [CrossRef]
13. Komerska, A.; Bianco, L.; Serra, V.; Fantucci, S.; Rosinski, M. Experimental analysis of an external dynamic solar shading integrating PCMs: First results. *Energy Procedia* **2015**, *78*, 3452–3457. [CrossRef]
14. Aelenei, L.; Aelenei, D.; Romano, R.; Mazzucchelli, E.S.; Brzezicki, M.; Rico-Martinez, J.M. *Case Studies—Adaptive Façade Network*; TU Delft Open: Delft, The Netherlands, 2018.
15. Al Dakheel, J.; Tabet Aoul, K. Building Applications, Opportunities and Challenges of Active Shading Systems: A State-of-the-Art Review. *Energies* **2017**, *10*, 1672. [CrossRef]
16. Premier, A. Solar shading devices integrating smart materials: An overview of projects, prototypes and products for advanced facade design. *Archit. Sci. Rev.* **2019**, *62*, 455–465. [CrossRef]
17. Brzezicki, M. A Systematic Review of the Most Recent Concepts in Kinetic Shading Systems with a Focus on Biomimetics: A Motion/Deformation Analysis. *Sustainability* **2024**, *16*, 5697. [CrossRef]
18. Chan, Y.C.; Tzempelikos, A. Daylighting and energy analysis of multi-sectional facades. *Energy Procedia* **2015**, *78*, 189–194. [CrossRef]
19. Lee, D.-S.; Koo, S.-H.; Seong, Y.-B.; Jo, J.-H. Evaluating Thermal and Lighting Energy Performance of Shading Devices on Kinetic Façades. *Sustainability* **2016**, *8*, 883. [CrossRef]
20. Sheikh, W.T.; Asghar, Q. Adaptive biomimetic facades: Enhancing energy efficiency of highly glazed buildings. *Front. Archit. Res.* **2019**, *8*, 319–331. [CrossRef]
21. Damian, A.; Filip, R.G.; Catalina, T.; Frunzulica, R.; Notton, G. The influence of solar-shading systems on an office building cooling load. In Proceedings of the 7th International Conference on Energy Efficiency and Agricultural Engineering 2020, Ruse, Bulgaria, 12–14 November 2020.
22. Luan, L.T.; Thang, L.D.; Hung, N.M.; Nguyen, Q.H.; Nguyen-Xuan, H. Optimal design of an Origami-inspired kinetic facade by balancing composite motion optimization for improving daylight performance and energy efficiency. *Energy* **2021**, *219*, 119557. [CrossRef]
23. Hosseini, S.M.; Fadli, F.; Mohammadi, M. Biomimetic kinetic shading facade inspired by tree morphology for improving occupant's daylight performance. *J. Daylighting* **2021**, *8*, 65–82. [CrossRef]
24. Sankaewthong, S.; Horanont, T.; Miyata, K.; Karnjana, J.; Busayarat, C.; Xie, H. Using a Biomimicry Approach in the Design of a Kinetic Façade to Regulate the Amount of Daylight Entering a Working Space. *Buildings* **2022**, *12*, 2089. [CrossRef]
25. Anzaniyan, E.; Alaghmandan, M.; Koohsari, A.M. Design, fabrication and computational simulation of a bio-kinetic facade inspired by the mechanism of the *Lupinus succulentus* plant for daylight and energy efficiency. *Sci. Technol. Built Environ.* **2022**, *28*, 1456–1471. [CrossRef]
26. Mangkuto, R.A.; Koerniawan, M.D.; Apriliyanthi, S.R.; Lubis, I.H.; Atthaillah; Hensen, J.L.M.; Paramita, B. Design Optimisation of Fixed and Adaptive Shading Devices on Four Façade Orientations of a High-Rise Office Building in the Tropics. *Buildings* **2022**, *12*, 25. [CrossRef]

27. Catto Lucchino, E.; Goia, F. Multi-domain model-based control of an adaptive façade based on a flexible double skin system. *Energy Build.* **2023**, *285*, 112881. [CrossRef]
28. Shen, L.; Han, Y. Optimizing the modular adaptive façade control strategy in open office space using integer programming and surrogate modelling. *Energy Build.* **2022**, *254*, 111546. [CrossRef]
29. Ożadowicz, A.; Walczyk, G. Energy Performance and Control Strategy for Dynamic Façade with Perovskite PV Panels—Technical Analysis and Case Study. *Energies* **2023**, *16*, 3793. [CrossRef]
30. de Bem, G.; Krüger, E.; La Roche, P.; de Abreu, A.A.A.M.; Luu, L. Development of ReShadS, a climate-responsive shading system: Conception, design, fabrication, and small-scale testing. *J. Build. Eng.* **2024**, *89*, 109423. [CrossRef]
31. Kim, J.H.; Han, S.H. Indoor Daylight Performances of Optimized Transmittances with Electrochromic-Applied Kinetic Louvers. *Buildings* **2022**, *12*, 263. [CrossRef]
32. Norouziasas, A.; Tabadkani, A.; Rahif, R.; Amer, M.; van Dijk, D.; Lamy, H.; Attia, S. Implementation of ISO/DIS 52016-3 for adaptive façades: A case study of an office building. *Build. Environ.* **2023**, *235*, 110195. [CrossRef]
33. Naeem, N.; Abdin, A.; Saleh, A. An Approach to Using Shape Memory Alloys in Kinetic Façades to Improve the Thermal Performance of Office Building Spaces. *Civ. Eng. Archit.* **2024**, *12*, 326–349. [CrossRef]
34. Vazquez, E.; Duarte, J.P. Bistable kinetic shades actuated with shape memory alloys: Prototype development and daylight performance evaluation. *Smart Mater. Struct.* **2022**, *31*, 34001. [CrossRef]
35. Carlucci, F.; Loonen, R.C.G.M.; Fiorito, F.; Hensen, J.L.M. A Novel Approach to Account for Shape-Morphing and Kinetic Shading Systems in Building Energy Performance Simulations. *J. Build. Perform. Simul.* **2022**, *16*, 346–365. [CrossRef]
36. Reinhart, C.F.; Walkenhorst, O. Validation of dynamic radiance-based daylight simulations for a test office with external blinds. *Energy Build.* **2001**, *33*, 683–697. [CrossRef]
37. Ng, K.M.; Adam, N.M.; Ab Kadir, M.Z.A. Experimental investigation of shading facade-integrated solar absorber system under hot tropical climate. *J. Build. Eng.* **2019**, *23*, 136–143. [CrossRef]
38. Yoon, Y.; Moon, J.W.; Kim, S. Development of annual daylight simulation algorithms for prediction of indoor daylight illuminance. *Energy Build.* **2016**, *118*, 1–17. [CrossRef]
39. Kharvari, F. An empirical validation of daylighting tools: Assessing radiance parameters and simulation settings in Ladybug and Honeybee against field measurements. *Sol. Energy* **2020**, *207*, 1021–1036. [CrossRef]
40. Reinhart, C.F.; Andersen, M. Development and validation of a radiance model for a translucent panel. *Energy Build.* **2006**, *38*, 890–904. [CrossRef]
41. Reinhart, C.F. *Daylighting Handbook II*; Building Technology Press: Cambridge, MA, USA, 2018.
42. Do, C.T.; Chan, Y.C. Evaluation of the effectiveness of a multi-sectional facade with Venetian blinds and roller shades with automated shading control strategies. *Sol. Energy* **2020**, *212*, 241–257. [CrossRef]
43. Ladybug Tools Community. Sub-Annual Daylight Simulation with Timestep Other Than 1. Ladybug Tools Discourse. Available online: https://discourse.ladybug.tools/t/sub-annual-daylight-simulation-with-timestep-other-than-1/17247 (accessed on 26 August 2024).
44. Ladybug Tools. 2024. EPW Map. Available online: https://www.ladybug.tools/epwmap/ (accessed on 1 June 2024).
45. Nabil, A.; Mardaljevic, J. Useful daylight illuminance: A new paradigm for assessing daylight in buildings. *Light. Res. Technol.* **2005**, *37*, 41–59. [CrossRef]
46. Boubekri, M.; Lee, J. A comparison of four daylighting metrics in assessing the daylighting performance of three shading systems. *J. Green Build.* **2017**, *12*, 39–53. [CrossRef]
47. Wienold, J.; Christoffersen, J. Evaluation methods and development of a new glare prediction model for daylight environments with the use of CCD cameras. *Energy Build.* **2006**, *38*, 743–757. [CrossRef]
48. Mandalaki, M.; Tsoutsos, T. *Solar Shading Systems: Design, Performance, and Integrated Photovoltaics*; Springer International Publishing AG: Berlin/Heidelberg, Germany, 2019.
49. Bahdad, A.A.S.; Fadzil, S.F.S.; Taib, N. Optimization of Daylight Performance Based on Controllable Light-shelf Parameters using Genetic Algorithms in the Tropical Climate of Malaysia. *J. Daylighting* **2020**, *7*, 122–136. [CrossRef]
50. Zazzini, P.; Romano, A.; Di Lorenzo, A.; Portaluri, V.; Di Crescenzo, V. Experimental Analysis of the Performance of Light Shelves in Different Geometrical Configurations Through the Scale Model Approach. *J. Daylighting* **2020**, *7*, 37–56. [CrossRef]
51. Ambient Light Sensor IC Series. Digital 16bit Serial Output Type Ambient Light Sensor IC. Rohm Semiconductors. Technical Note. BH-1750 FVI. Available online: https://fscdn.rohm.com/en/products/databook/datasheet/ic/sensor/light/bh1721fvc_spec-e.pdf (accessed on 1 June 2024).
52. Markowicz, K.M.; Stachlewska, I.S.; Zawadzka-Manko, O.; Wang, D.; Kumala, W.; Chilinski, M.T.; Makuch, P.; Markuszewski, P.; Rozwadowska, A.K.; Petelski, T.; et al. A Decade of Poland-AOD Aerosol Research Network Observations. *Atmosphere* **2021**, *12*, 1583. [CrossRef]
53. Normy Klimatyczne 1991–2020—Portal Klimat IMGW-PiB. Available online: https://klimat.imgw.pl/pl/climate-normals/PPP_S (accessed on 1 June 2024).
54. Al-Obaidi, K.M.; Al-Duais, H.S.; Alduais, N.A.M.; Alashwal, A.; Ismail, M.A. Exploring the environmental performance of liquid glass coating using Sol-Gel technology and responsive Venetian blinds in the tropics. *J. Build. Eng.* **2022**, *62*, 105329. [CrossRef]
55. Duffie, J.A.; Beckman, W.A. *Solar Engineering of Thermal Processes*, 4th ed.; John Wiley & Sons: Hoboken, NJ, USA, 2013.

56. Han, S. Implementation and the energy efficiency of the kinetic shading system. *J. Korean Inst. Ecol. Archit. Environ.* **2014**, *14*, 67–73. [CrossRef]
57. Lee, B. Heating, Cooling, and Lighting Energy Demand Simulation Analysis of Kinetic Shading Devices with Automatic Dimming Control for Asian Countries. *Sustainability* **2019**, *11*, 1253. [CrossRef]
58. Bupi, A.; Kittisontirak, S.; Chinnavornrungsee, P.; Songtrai, S.; Manosukritkul, P.; Sriprapha, K.; Titiroongruang, W.; Niemcharoen, S. A Method to Improve the Accuracy of Simulation Models: A Case Study on Photovoltaic System Modelling. *Energies* **2021**, *14*, 372. [CrossRef]
59. Loutzenhiser, P.; Maxwell, G.; Manz, H. An Empirical Validation of the Daylighting Algorithms and Associated Interactions in Building Energy Simulation Programs Using Various Shading Devices and Windows. *Energy* **2007**, *32*, 1855–1870. [CrossRef]
60. Mazzeo, D.; Matera, N.; Cornaro, C.; Oliveti, G.; Romagnoni, P.; Santoli, L. EnergyPlus, IDA ICE and TRNSYS Predictive Simulation Accuracy for Building Thermal Behaviour Evaluation by Using an Experimental Campaign in Solar Test Boxes with and without a PCM Module. *Energy Build.* **2020**, *212*, 109812. [CrossRef]
61. Wang, Y.; Lv, Z.; Wang, Q.; Zhu, M.; Wang, F. Numerical Study on Heat Transfer Characteristics of Spray Cooling Double Skin Façade. *Appl. Therm. Eng.* **2024**, *241*, 122392. [CrossRef]
62. Takhmasib, M.; Lee, H.J.; Yi, H. Machine-learned kinetic Façade: Construction and artificial intelligence enabled predictive control for visual comfort. *Autom. Constr.* **2023**, *156*, 105093. [CrossRef]
63. Cacabelos, P.; Eguía, L.; Febrero, E.; Granada, E. Development of a new multi-stage building energy model calibration methodology and validation in a public library. *Energy Build.* **2017**, *146*, 182–199. [CrossRef]
64. Ascione, F.; Bianco, N.; Böttcher, O.; Kaltenbrunner, R.; Vanoli, G.P. Net zero-energy buildings in Germany: Design, model calibration and lessons learned from a case study in Berlin. *Energy Build.* **2016**, *133*, 688–710. [CrossRef]
65. Royapoor, M.; Roskilly, T. Building model calibration using energy and environmental data. *Energy Build.* **2015**, *94*, 109–120. [CrossRef]
66. ASHRAE, ASHRAE Guideline. *Guideline 14-2014: Measurement of Energy, Demand, and Water Savings*; American Society of Heating, Refrigerating, and Air Conditioning Engineers: Atlanta, Georgia, 2014.

Disclaimer/Publisher's Note: The statements, opinions and data contained in all publications are solely those of the individual author(s) and contributor(s) and not of MDPI and/or the editor(s). MDPI and/or the editor(s) disclaim responsibility for any injury to people or property resulting from any ideas, methods, instructions or products referred to in the content.